Comparison of the dynamics of exoskeletal-assisted and unassisted locomotion in an FDA-approved lower extremity device: Controlled experiments and development of a subject-specific virtual simulator

Vishnu D. Chandran[1], Sanghyun Nam[1], David Hexner[2], William A. Bauman[3,4], and Saikat Pal[1,5]

[1]Department of Biomedical Engineering, New Jersey Institute of Technology, Newark, NJ

[2]ReWalk Robotics, Yokneam, Israel

[3]James J. Peters Veterans Affairs Medical Center, Bronx, NY, USA

[4]Department of Medicine and Rehabilitation & Human Performance, Icahn School of Medicine at Mount Sinai

[5]Department of Electrical and Computer Engineering, New Jersey Institute of Technology, Newark, NJ

* Corresponding author

Email: pal@njit.edu (SP)

Abstract

Robotic exoskeletons have considerable, but largely untapped, potential to restore mobility in individuals with neurological disorders, and other conditions that result in partial or complete immobilization. The growing demand for these devices necessitates the development of technology to characterize the human-robot system during exoskeletal-assisted locomotion (EAL) and accelerate robot design refinements. The goal of this study was to combine controlled experiments with computational modeling to build a virtual simulator of EAL. The first objective was to acquire a minimum empirical dataset comprising human-robot kinematics, ground reaction forces, and electromyography during exoskeletal-assisted and unassisted locomotion from an able-bodied participant. The second objective was to quantify the dynamics of the human-robot system using a subject-specific virtual simulator reproducing EAL compared to the dynamics of normal gait. We trained an able-bodied participant to ambulate independently in a Food and Drug Administration-approved exoskeleton, the ReWalk P6.0 (ReWalk Robotics, Yoknaem, Israel). We analyzed the motion of the participant during exoskeletal-assisted and unassisted walking, sit-to-stand, and stand-to-sit maneuvers, with simultaneous measurements of (i) three-dimensional marker trajectories, (ii) ground reaction forces, (iii) electromyography, and (iv) exoskeleton encoder data. We created a virtual simulator in OpenSim, comprising a whole-body musculoskeletal model and a full-scale exoskeleton model, to determine the joint kinematics and moments during exoskeletal-assisted and unassisted maneuvers. Mean peak knee flexion angles of the human subject during exoskeletal-assisted walking were 50.1° ± 0.6° (left) and 52.6° ± 0.7° (right), compared to 68.6° ± 0.3° (left) and 70.7° ± 1.1° (right) during unassisted walking. Mean peak knee extension moments during exoskeletal-assisted walking were 0.10 ± 0.10 Nm/kg (left) and 0.22 ± 0.11 Nm/kg (right), compared to 0.64 ± 0.07 Nm/kg (left) and 0.73

40 ± 0.10 Nm/kg (right) during unassisted walking. This work provides a foundation for parametric
41 studies to characterize the effects of human and robot design variables, and predictive modeling
42 to optimize human-robot interaction during EAL.
43

Introduction

Wearable robotic exoskeletons have considerable potential to transform the people's lives by reducing the metabolic cost of walking [1-3], carrying heavy loads [4, 5], or augmenting human performance to conduct strenous tasks over extended periods of time [6, 7]. The need for such assistive devices is particularly profound in restoring mobility in individuals with neurological disorders, including those of spinal cord injury, stroke, traumatic brain injury, and multiple sclerosis. Wearable robotic exoskeletons for rehabilitation of individuals with neurological disorders are relatively new. The ReWalk (ReWalk Robotics, Yoknaem, Israel) was the first lower extremity device to receive Food and Drug Administration (FDA) approval in 2014, followed by the Ekso (Ekso Bionics, Richmond, CA) and Indego (Parker Hannifin, Cleveland, OH) in 2016, and the Keeogo (B-temia Inc., Quebec City, Canada) in 2020. Prior studies have demonstrated the ability of individuals with neurological disorders who have partial impairments to those who are completely non-ambulatory to walk independently in robotic exoskeletons [8-19]. Exoskeletal-assisted locomotion (EAL) has been shown to improve functional and motor recovery [8], mobility [9, 10, 15, 16], chronic pain [20], muscle spasticity [20-22], cardiovascular health [13, 23], bowel function [24], bladder function [21, 22], and quality of life [21]. These studies highlight the growing demand for wearable robotic exoskeletons to improve physical and psychological health, employment opportunities, and community integration in persons with neurological disorders.

The growing demand for wearable robotic exoskeletons for rehabilitation of individuals with neurological disorders has exposed two gaps in knowledge. First, the dynamics (comprising joint kinematics and joint kinetics) of the human-robot system during EAL in FDA-approved devices are not well-understood. The human-robot entity during EAL represents a complex

dynamic system, and parsing out the contributions of the human from the robot, together with their interaction effects, requires a minimum empirical dataset that includes human-robot kinematics, ground reaction forces, and electromyography (EMG). Such a dataset from EAL in an FDA-approved device does not exist. Kim and colleagues quantified the dynamics of the human-robot system during EAL in a device designed to augment human performance in industrial settings [25]; however, this exoskeleton is not FDA-approved for rehabilitation of individuals with neurological disorders. Previous studies with FDA-approved exoskeletons for neurological disorders have reported joint kinematics [10, 26-28], EMG [10, 29, 30], and foot reaction forces from pressure insoles [14]. To the best of our knowledge, no prior study has reported joint kinetics of the human-robot system during EAL in an FDA-approved device. Furthermore, a minimum empirical dataset comprising joint kinematics, ground reaction forces, and EMG from a single session of controlled experiments with and without an FDA-approved exoskeleton is not available in the literature.

The second gap in knowledge exposed by the growing demand for wearable robotic exoskeletons is that existing technology to accelerate design refinements and improve human experience in these devices is extremely limited. It is not ethically feasible, and would undoubtedly be prohibitively expensive, to conduct a large number of human experiments to characterize the effects of an endless number of robot design variables, control strategies, and human parameters on the human-robot system during EAL. Computational simulation is a viable alternative to perform such parametric studies. Prior studies have used computational simulations of the human-robot system to optimize exoskeleton design [31-35], test control strategies [36-39], minimize the metabolic cost of locomotion [40-42], optimize assistance for pathological gait

[43, 44], and study human-robot interaction [45-50]. However, no prior study has simulated EAL in an FDA-approved exoskeleton.

The goal of this study was to combine controlled experiments with computational modeling to build a virtual simulator of EAL in an FDA-approved lower extremity exoskeleton, the ReWalk P6.0. The first objective of this study was to acquire a minimum empirical dataset comprising human-robot kinematics, ground reaction forces, and EMG during exoskeletal-assisted and unassisted locomotion. The second objective of this study was to quantify the dynamics of the human-robot system using a subject-specific virtual simulator reproducing EAL compared to the dynamics of normal gait.

Methods

Participant recruitment

We recruited an able-bodied participant (age in their 40s, male, height 1.76 m, mass 89.4kg) for this study. The inclusion criteria were age between 18-55 years, height between 1.60-1.90 meters, and weight <90 kg, body mass index between 18.5-29.9 kg/m^2, no known history of musculoskeletal disease or dysfunction, normal range of motion of the lower extremities, and willingness to commit to exoskeleton training for five sessions followed by one session of motion capture experiment performing exoskeletal-assisted and unassisted locomotion. The exclusion criteria were known history of musculoskeletal surgeries or non-surgical interventions, inability to hold crutches, pregnant, lactating, or menopausal. The participant was informed on all aspects of the study and provided informed signed consent according to the policies of our Institutional Review Board.

Exoskeletal-assisted locomotion training

The participant was trained to perform sit-to-stand, stand-to-sit, and walking maneuvers in the ReWalk P6.0. Prior to initiating training, the exoskeleton was adjusted to fit the anthropometry of the participant, including pelvic band size, thigh leg length, shank leg length, knee bracket position, foot plate size, and ankle dorsiflexion setting [51]. Walking in the ReWalk P6.0 follows a standard procedure. To initiate walking in the ReWalk P6.0, the user starts in the standing position with the hand crutches on each side. The user activates the “Walk” mode through a controller watch, which is confirmed by a single beep. To perform the device-assisted gait maneuver, the user unweights each side in an alternating manner—that is, the right leg is unloaded by leaning the torso to the left, which is followed by leaning the torso to the right, which unloads the left leg, and so forth. The action of the user swaying from side-to-side and, thereby, unloading the contralateral leg, activates the hip and knee motors to initiate the stepping motion. The next several steps are a repetition of the back-and-forth swaying of the torso to unload the trailing leg to permit the stepping action to continue.

The sit-to-stand and stand-to-sit maneuvers in the ReWalk P6.0 follow standard procedures. To initiate the sit-to-stand maneuver, a user places the hand crutches posterior to the hip while seated. Then, the trainer activates the “Stand” mode through a controller, which is confirmed by a single beep. The hip motors flex the torso (~9°) to position the user’s upper body forward while they load the crutches. The user has to hold this position for 3 seconds, after which time the exoskeleton beeps thrice and activates the hip and knee motors to complete the sit-to-stand maneuver. Next, the stand-to-sit maneuver in the ReWalk P6.0 follows a similar procedure. A user places the hand crutches posterior to the hip while standing. Then, the trainer activates the “Sit” mode, which is confirmed by a single beep. The user gets into position by

leaning backward (~6°) and loading the crutches. The user has to hold this position for 3 seconds, after which time the exoskeleton beeps thrice and activates the hip and knee motors to complete the stand-to-sit maneuver. By the end of the fourth 1-hour session, the participant was able to perform the sit-to-stand, stand-to-sit, and walking maneuvers in the exoskeleton independent of requiring any assistance.

Motion capture experiments during exoskeletal-assisted and unassisted locomotion

We analyzed the participant during exoskeletal-assisted and unassisted locomotion from a single motion capture session, including simultaneous measurements of three-dimensional (3-D) marker trajectories, ground reaction forces, EMG, and exoskeleton encoder data. A 16-camera motion capture system (Vicon V8 and Nexus, Vicon Motion Systems, Oxford, UK) was used to track retro-reflective markers at 100 Hz. The markers were placed on the participant and the exoskeleton to capture the position and orientation of all the human body and exoskeleton segments (Figs 1A and 1B). The markers were placed on the participant according to the Conventional Gait Model 2.5 template in Vicon Nexus [52]. Markers were placed on the exoskeleton based on a custom template (Figs 1A and 1B). Next, we recorded ground reaction forces from each foot using four overground force plates (Bertec Corp., Columbus, OH) sampled at 2000 Hz. The force data were filtered using a low-pass, fourth-order Butterworth filter with a cutoff frequency of 15 Hz.

Fig 1. (A, B) Placement of retro-reflective markers on the human (blue, cyan, and red), exoskeleton (yellow), and crutches (green) to track the position and orientation of all the

158 segments of the human-robot system. The blue and cyan markers represent the Conventional
159 Gait Model (CGM) 2.5 marker set, with the cyan markers removed after initial calibration. The
160 red markers are offset markers used to locate occluded anatomical landmarks when the
161 participant is in the exoskeleton. During post-processing, the occluded anatomical landmarks are
162 reconstructed using these offset markers to complete the CGM 2.5 marker set. Next, we created a
163 custom template to track the different segments of the exoskeleton and crutches. (C) The human-
164 robot model in the virtual simulator comprises a universal joint (six degrees of freedom) at the
165 pelvic band to anchor the exoskeleton to the participant, and a pin joint (one degree of freedom)
166 each at the hips and knees of the exoskeleton. The location of the different joint axes are shown.
167 (D) A generic musculoskeletal [53] was scaled to the participant's anthropometry.
168
169 We recorded muscle EMG measurements from both legs using a 16-channel surface
170 system (Trigno^{TM}, Delsys Inc., Natick, MA) sampled at 2000 Hz. We measured EMG from
171 rectus femoris, vastus lateralis, vastus medialis, semitendinosus, biceps femoris, gastrocnemius
172 medialis, soleus, and tibialis anterior muscles using established protocols [54, 55]. The
173 participant's mean resting EMG was determined from unassisted standing trials with the
174 participant instructed to remain stationary in a neutral pose with their muscles relaxed. The mean
175 resting EMG value was subtracted from their raw EMG values from the locomotion trials to
176 offset the data to zero. We filtered the EMG data using a fourth-order high-pass filter (30 Hz) to
177 remove motion artifact and then full-wave rectified and filtered with a fourth-order Butterworth
178 low-pass filter (6 Hz) to obtain the linear envelope of muscle activation [56]. The filtered EMG
179 data were normalized to muscle-specific activations obtained from maximum voluntary
180 contraction trials. In addition, we recorded exoskeleton encoder data from all motion capture

trials, including timestamps corresponding to the activation of the motors and motor encoder angles. These data were synchronized with the 3-D marker trajectory, ground reaction force, and EMG data.

Motion capture of exoskeletal-assisted and unassisted walking

We acquired 3-D motion data while the participant walked back and forth over a 5.0 x 2.5 m even instrumented walkway with and without the exoskeleton. The participant walked 10 times back and forth with the exoskeleton at the participant's preferred speed (0.47 ± 0.03 m/s), and 10 times unassisted at self-selected speed (1.11 ± 0.07 m/s). From this dataset, only successful trials were included for further analysis. A walking trial was determined as successful if the foot placements were entirely on single force plates and there were no missing marker, ground reaction force, and EMG data. Additional criteria for a successful trial during exoskeletal-assisting walking was that the hand crutches were placed away from the force plates so as not to interfere with the ground reaction forces from the feet and there were no missing exoskeleton encoder data. Based on these criteria, we obtained six successful trials each of exoskeletal-assisted and unassisted walking.

Motion capture of exoskeletal-assisted and unassisted sit-to-stand and stand-to-sit maneuvers

We acquired 3-D motion data while the participant performed sit-to-stand and stand-to-sit maneuvers with and without the exoskeleton. The participant used an armless piano bench with seat height of 43 cm positioned on the overground walkway that enabled each foot to be placed on a force plate during the entire duration of a maneuver. The participant performed the sit-to-

stand and stand-to-sit maneuvers 10 times each with and without the exoskeleton. From this dataset, only successful trials were included for further analysis. A trial was determined as successful if the foot placements were entirely on single force plates and there were no missing marker, ground reaction force, and EMG data. Additional criteria for a successful trial during exoskeletal-assisting sit-to-stand/stand-to-sit were that the hand crutches were placed away from the force plates so as not to interfere with the ground reaction forces from the feet and there were no missing exoskeleton encoder data. Based on these criteria, we obtained four and five successful trials of exoskeletal-assisted and unassisted sit-to-stand maneuvers, respectively, and five successful trials each of exoskeletal-assisted and unassisted stand-to-sit maneuvers.

Virtual simulator reproducing exoskeletal-assisted and unassisted locomotion

We developed a virtual simulator in OpenSim [57] to reproduce exoskeletal-assisted and unassisted walking, sit-to-stand, and stand-to-sit maneuvers (Fig 1C-D). We integrated a previously published human musculoskeletal model [53] with a full-scale model of the ReWalk P6.0 exoskeleton. The musculoskeletal model comprised 24 segments and 37 degrees of freedom (DoFs): seven in each leg, six at the pelvis, three at the torso, and seven in each arm [53]. The seven DoFs in each leg included three DoFs at the ball-and-socket hip joint, a one DoF coupled knee mechanism with translations of the tibia and patella prescribed by the knee flexion angle, and one DoF revolute joints at the ankle, subtalar, and metatarsal joints. A six DoF universal joint at the pelvis was used to describe the pose of the musculoskeletal model with respect to the global origin. The three DoFs in the torso and upper body included a spherical joint connecting the torso to the pelvis. The seven DoFs in each arm included three DoFs at the ball-and-socket

shoulder joint, one DoF revolute joint at the elbow, one DoF revolute joint between the radius and the ulna, and two DoFs universal joint between the radius and the hand for wrist flexion-extension and radial-ulnar deviation. The full-scale model of the exoskeleton comprised seven segments and four DoFs (Fig 1C). The four DoFs included a single DoF pin joint each at the hips and knees of the exoskeleton. The ankle joints in the exoskeleton were welded to the lower leg segments. Next, human-robot interactions were modeled using an additional six DoF universal joint at the pelvic band to anchor the exoskeleton to the participant (Fig 1C). The musculoskeletal model included 80 Hill-type muscle-tendon units [58]. The Hill-type muscle-tendon units captured the force-length-velocity properties of the lower extremity muscles, with muscle geometry and architecture based on adult cadaver data [59].

We adapted a previously published computational framework in OpenSim [53, 60] to determine the dynamics of exoskeletal-assisted and unassisted walking, sit-to-stand, and stand-to-sit maneuvers. We scaled the generic musculoskeletal model to match the mass and segment lengths of the participant. We determined joint kinematics by performing Inverse Kinematics (IK) analyses in OpenSim. IK solves for kinematics by minimizing error between the experimentally measured marker positions and the corresponding markers on the human-robot model. We performed Inverse Dynamics (ID) analyses to compute net human-robot joint torques. For ID analyses, we simplified the human-robot model by incorporating the mass and inertial properties of the exoskeleton with the musculoskeletal segments, similar to previous studies [61, 62]. Exoskeleton masses were added to the respective segments in the musculoskeletal model. The centers of mass of the segments in the musculoskeletal model were moved to the locations corresponding to the combined human-robot segments.

Data analysis and statistical methods

We compared hip, knee, and ankle flexion-extension angles from each leg during exoskeletal-assisted and unassisted walking, sit-to-stand, and stand-to-sit maneuvers. For exoskeletal-assisted maneuvers, we determined the hip and knee flexion-extension angles from the robot using IK and exoskeleton encoder data; the RMS errors between these two methods were minimal (the worst case was 3.3°), as such only joint angles from IK are presented in this study. The joint angles from multiple trials were averaged for each leg. We compared the vertical, anterior-posterior (AP), and medial-lateral (ML) ground reaction forces from each leg during exoskeletal-assisted and unassisted walking, sit-to-stand, and stand-to-sit maneuvers. The ground reaction forces from EAL were normalized to the combined weight of the participant and the exoskeleton; forces from unassisted locomotion were normalized to the participant's body weight. Ground reaction forces from multiple trials were averaged for each leg. Next, we compared normalized EMG from the eight lower extremity muscles from each leg during exoskeletal-assisted and unassisted walking, sit-to-stand, and stand-to-sit maneuvers. Normalized EMG from multiple trials were averaged for each leg. Finally, we compared hip, knee, and ankle moments from each leg during exoskeletal-assisted and unassisted walking, sit-to-stand, and stand-to-sit maneuvers. The joint moments from EAL were normalized to the combined mass of the participant and the exoskeleton; joint moments from unassisted locomotion were normalized to the participant's mass. The joint moments from multiple trials were averaged for each leg.

Results

Exoskeletal-assisted and unassisted walking

The virtual simulator reproduced exoskeletal-assisted and unassisted walking within acceptable tolerances, with average RMS errors between experiment and simulator markers being 1.3 cm and 1.2 cm for exoskeletal-assisted and unassisted trials, respectively. We observed differences in joint kinematics between exoskeletal-assisted and unassisted walking (Fig 1). Mean peak hip extension angles of the human during exoskeletal-assisted walking were 3.1° ± 1.9° (left) and 0.2° ± 0.9° (right), compared to 27.2° ± 1.2° (left) and 25.1° ± 1.0° (right) during unassisted walking (Figs 2A and 2B). After subtracting the offset angles due to different definitions of coordinate axes, average absolute difference between human and robot hip flexion-extension angles were 1.5° ± 1.4° (left) and 1.9° ± 1.0° (right). Mean peak knee flexion angles of the participant during exoskeletal-assisted walking were 50.1° ± 0.6° (left) and 52.6° ± 0.7° (right), compared to 68.6° ± 0.3° (left) and 70.7° ± 1.1° (right) during unassisted walking (Figs 2C and 2D). After subtracting the offset angles, average absolute difference between participant and robot mean knee flexion-extension angles were 1.7° ± 1.1° (left) and 0.8° ± 0.5° (right). Mean peak ankle plantarflexion angles of the participant during exoskeletal-assisted walking were 6.9° ± 2.8° (left) and 6.7° ± 3.9° (right), compared to 13.9° ± 2.5° (left) and 19.5° ± 1.9° (right) during unassisted walking (Figs 2E and 2F). Peak plantarflexion during exoskeletal-assisted walking occurred in early stance during braking, in contrast to peak plantarflexion at the end of propulsion (toe-off) during unassisted walking. We observed a minimal range of plantarflexion (5.3°-10.5°) in the propulsion phase during exoskeletal-assisted walking, compared to a larger range (27.1°- 30.3°) during unassisted walking.

Fig 2. Average (±1 SD) hip (A, B), knee (C, D), and ankle (E, F) joint angles from six exoskeletal-assited (human: blue for left leg, red for right leg; robot: black) and six unassisted (human: grey) walking trials. The offset in angles between the participant (blue or red) and the robot (black) was due to different definitions of coordinate axes for each rigid body. The dashed vertical lines represent toe-off.

We observed differences in normalized ground reaction forces between exoskeletal-assisted and unassisted walking, especially during the braking and propulsion phases (Fig 3). Mean peak vertical ground reaction forces during braking were 0.91 ± 0.08 BW (left) and 0.89 ± 0.06 BW (right) during exoskeletal-assisted walking, compared to 1.09± 0.02 BW (left) and 1.05 ± 0.05 BW (right) during unassisted walking (Figs 3A and 3B). Mean peak vertical ground reaction forces during propulsion were 0.98 ± 0.02 BW (left) and 1.02 ± 0.02 BW (right) during exoskeletal-assisted walking, compared to 1.04 ± 0.04 BW (left) and 1.02 ± 0.02 BW (right) during unassisted walking (Figs 3A and 3B). Mean peak posterior ground reaction forces during braking were 0.08 ± 0.04 BW (left) and 0.08 ± 0.02 BW (right) during exoskeletal-assisted walking, compared to 0.17 ± 0.01 BW (left) and 0.17 ± 0.04 BW (right) during unassisted walking (Figs 3C and 3D). Mean peak anterior ground reaction forces during propulsion were 0.06 ± 0.02 BW (left) and 0.08 ± 0.06 BW (right) during exoskeletal-assisted walking, compared to 0.18 ± 0.01 BW (left) and 0.19 ± 0.01 BW (right) during unassisted walking (Figs 3C and 3D). Mean peak lateral ground reaction forces during braking were 0.07 ± 0.02 BW (left) and 0.06 ± 0.01 BW (right) during exoskeletal-assisted walking, compared to 0.09 ± 0.01 BW (left) and 0.09 ± 0.01 BW (right) during unassisted walking (Figs 3E and 3F). Mean peak lateral ground reaction forces during propulsion 0.06 ± 0.01 BW (left) and 0.07 ± 0.01 BW (right)

317 during exoskeletal-assisted walking, compared to 0.08 ± 0.01 BW (left) and 0.10 ± 0.01 BW
318 (right) during unassisted walking (Figs 3E and 3F). The decreased ground reaction forces during
319 the braking and propulsion phases of exoskeletal-assisted walking were supported by EMG data
320 (Fig 4). The tibialis anterior muscle, used for braking, was less active during the braking and
321 terminal swing (to prepare for braking) phases during exoskeletal-assisted compared to
322 unassisted walking (Figs 4O and 4P). The gastrocnemius medialis and soleus muscles, used for
323 propulsion, were less active during the propulsion phase during exoskeletal-assisted compared to
324 unassisted walking (Figs 4K-4N).
325
326 **Fig 3.** Average (±1 SD) vertical (A, B), anterior-posterior (C, D) and medial-lateral (E, F)
327 ground reaction forces from six exoskeletal-assisted and six unassisted walking trials. The
328 ground reaction forces from EAL were normalized to the combined weight of the participant and
329 the exoskeleton; forces from unassisted locomotion were normalized to the participant's body
330 weight (BW). The dashed vertical lines represent toe-off.
331
332 **Fig 4.** Average (+1 SD) normalized electromyography (EMG) data from six exoskeletal-assisted
333 and six unassisted walking trials. The EMG data were normalized using muscle-specific
334 maximum voluntary contraction values. The dashed vertical lines represent toe-off.
335
336 We observed differences in joint moments between exoskeletal-assisted and unassisted
337 walking (Fig 5). Mean peak hip flexion moments of the participant during exoskeletal-assisted
338 walking 0.23 ± 0.05 Nm/kg (left) and 0.35 ± 0.06 Nm/kg (right), compared to 0.65 ± 0.07 Nm/kg
339 (left) and 0.64 ± 0.09 Nm/kg (right) during unassisted walking (Figs 5A and 5B). Mean peak

knee extension moments of the participant during exoskeletal-assisted walking were 0.10 ± 0.10 Nm/kg (left) and 0.22 ± 0.11 Nm/kg (right), compared to 0.64 ± 0.07 Nm/kg (left) and 0.73 ± 0.10 Nm/kg (right) during unassisted walking (Figs 5C and 5D). Mean peak ankle plantarflexion moments during exoskeletal-assisted walking were 0.80 ± 0.12 Nm/kg (left) and 0.78 ± 0.19 Nm/kg (right), compared to 1.29 ± 0.04 Nm/kg (left) and 1.12 ± 0.03 Nm/kg (right) during unassisted walking (Figs 5E and 5F).

Fig 5. Average (±1 SD) hip (A, B), knee (C, D), and ankle (E, F) joint moments from six exoskeletal-assited (human: blue for left leg, red for right leg) and six unassisted (human: grey) walking trials. The joint moments from EAL were normalized to the combined mass of the participant and the exoskeleton; joint moments from unassisted locomotion were normalized to the participant's mass. The dashed vertical lines represent toe-off.

Exoskeletal-assisted and unassisted sit-to-stand

The virtual simulator reproduced exoskeletal-assisted and unassisted sit-to-stand within acceptable tolerances, with average RMS errors between experiment and simulator markers being 1.5 cm and 1.9 cm for exoskeletal-assisted and unassisted trials, respectively. Exoskeletal-assisted sit-to-stand in the ReWalk P6.0 follows a standard procedure that is different from unassisted sit-to-stand, including different temporal events and phases. Comparison of exoskeletal-assisted and unassisted sit-to-stand is included as supplemental information, including joint kinematics (S1 Fig), ground reaction forces (S2 Fig), EMG (S3 Fig), and joint moments (S4 Fig).

Exoskeletal-assisted and unassisted stand-to-sit

The virtual simulator reproduced exoskeletal-assisted and unassisted stand-to-sit within acceptable tolerances, with average RMS errors between experiment and simulator markers being 1.4 cm and 1.9 cm for exoskeletal-assisted and unassisted trials, respectively. Exoskeletal-assisted stand-to-sit in the ReWalk P6.0 follows a standard procedure that is different from unassisted stand-to-sit, including different temporal events and phases. Comparison of exoskeletal-assisted and unassisted stand-to-sit is included as supplemental information, including joint kinematics (S5 Fig), ground reaction forces (S6 Fig), EMG (S7 Fig), and joint moments (S8 Fig).

Discussion

The goal of this study was to combine controlled experiments with computational modeling to build a virtual simulator of EAL in the ReWalk P6.0, an FDA-approved lower extremity exoskeleton for rehabilitation of patients with neurological disorders. The first objective of this study was to acquire a minimum empirical dataset comprising human-robot kinematics, ground reaction forces, and EMG during exoskeletal-assisted and unassisted locomotion. Here, we present a minimum empirical dataset from a single session of controlled experiments with an able-bodied participant performing exoskeletal-assisted and unassisted walking, sit-to-stand, and stand-to-sit maneuvers. Our results provide a direct comparison of joint kinematics (Fig 2, S1 Fig, and S5 Fig), ground reaction forces (Fig 3, S2 Fig, and S6 Fig), and EMG (Fig 4, S3 Fig, and S7 Fig) during exoskeletal-assisted and unassisted locomotion in an FDA-approved exoskeleton. The second objective of this study was to quantify the dynamics of the human-robot system using a subject-specific virtual simulator reproducing EAL, and to

compare with the dynamics of unassisted locomotion. The subject-specific virtual simulator reproduced EAL within acceptable tolerances (RMS errors of 1.2-1.3 cm for walking, 1.5-1.9 cm for sit-to-stand, and 1.4-1.9 cm for stand-to-sit maneuvers). Our results provide a direct comparison of joint moments during exoskeletal-assisted and unassisted locomotion in an FDA-approved exoskeleton (Fig 5, S4 Fig, and S8 Fig).

We are not aware of any prior literature that has provided a direct comparison of joint kinematics, ground reaction forces, EMG, and joint moments from a single session of controlled experiments with and without an FDA-approved exoskeleton. As such, we have compared our findings with data that is available in the literature. Our joint kinematics results from exoskeletal-assisted walking in the ReWalk P6.0 are comparable to those reported by Chang et al. using the Ekso device [28]. Our mean peak hip extension, knee flexion, and ankle plantarflexion angles were 0.2°-3.1°, 50.1°-52.6°, and 6.7°-6.9°, respectively (Fig 2); in comparison, mean peak hip extension, knee flexion, and ankle plantarflexion angles reported in Chang et al. are ~3.0°-4.0°, ~48.0°-50.0°, and ~6.0°-9.0°, respectively [28]. Ekelem et al. reported median peak hip and knee flexion angles of ~2.0°-16.0° and ~23.0°-25.0°, respectively, during exoskeletal-assisted walking in the Indego device [27]. Since they do not report peak hip extension angles during stance, a direct comparison with our hip extension angle data is not possible. Their peak knee flexion values (~23.0°-25.0°) are lower than our values (50.1°-52.6°). This is likely because the two participants in their study had high levels of spasticity; with functional electrical stimulation, they were able to increase the participants' peak knee flexion angles to ~35.0°-47.0° [27]. Our hip, knee, and ankle kinematics are in agreement with the results from Talaty et al., who also analyzed exoskeletal-assisted walking in the ReWalk [26]. Next, Fineberg et al. reported vertical ground reaction forces obtained from in-shoe pressure insoles (F-Scan, TekScan, Boston, MA)

during exoskeletal-assisted walking in the ReWalk device [14]; our vertical ground reaction forces are in agreement with Fineberg et al. There is no prior study to compare our measured anterior-posterior and medial-lateral ground reaction forces during EAL. Regarding muscle activity during EAL, Bellitto et al. compared EMG data from three incomplete spinal cord injured participants during exoskeletal-assisted (with the Ekso device) and unassisted walking [29]. The timings of our EMG activity are in agreement, but our normalized magnitudes are lower than those reported in Bellitto et al. This is likely because of two reasons: 1) our results are from an able-bodied participant, compared to incomplete spinal cord injured participants in Bellitto et al.; and 2) we normalized our EMG to maximum voluntary contraction data, while Bellitto et al. used a dynamic normalization technique [63], where EMG data from each muscle were normalized to the maximum value over all trials with and without the exoskeleton. There is no prior study to compare our results from sit-to-stand and stand-to-sit maneuvers.

This study provides a much-needed empirical dataset to develop virtual simulators reproducing EAL in FDA-approved devices. To the best of our knowledge, there is not a single virtual simulator of EAL in an FDA-approved exoskeleton. Prior studies have developed virtual simulators of EAL in custom-built exoskeletons [44-47, 49, 64], but these devices are not FDA-approved and are likely many years away from widespread application for the rehabilitation of patients with neurological disorders. Prior studies have also developed virtual simulators of EAL based on idealized or imaginary exoskeletons [37, 40-42, 48, 50]. For example, Bianco et al. developed a virtual simulator to examine how multi-joint assistance affects the metabolic cost of exoskeletal-assisted and unassisted walking [37]. This simulator, however, was not based on a physical exoskeleton and empirical data from unassisted walking was used as model inputs, with the assumption that joint kinematics, ground reaction forces, and EMG do not change between

exoskeletal-assisted and unassisted walking. They stated in their limitations that incorporating the kinematic adaptations due to an exoskeleton would alter their metabolic cost predictions. It is likely that Bianco et al. and other studies that developed virtual simulators based on idealized or imaginary exoskeletal-assistance did so because they did not have empirical data from EAL.

A potential limitation of this study is that the ReWalk P6.0 was designed for patients with spinal cord injury, but the results from this study were obtained from an able-bodied participant. These results provide new understanding of the dynamics of the human-robot system during EAL in an FDA-approved device. We anticipate building upon this work by analyzing participants with spinal cord injury. A second limitation of this study is that our EAL experiments did not measure the external crutch reaction forces or the interaction forces due to the knee brackets and straps that were used to secure the participant in the exoskeleton. These forces were also not included in the virtual simulator and, as such, their effects on our findings remain undefined. A third potential limitation is that we incorporated the mass and inertial properties of the exoskeleton with the musculoskeletal segments, similar to that reported in previous studies, and thus simplified our virtual simulator for ID analyses [61, 62]. A more thorough approach would have been to segregate the human and robot components, include human-robot interaction forces as input and to solve the human and robot kinematic chains separately.

This study provides a framework for determining the dynamics of the human-robot system during EAL in an FDA-approved exoskeleton using controlled experiments and a subject-specific virtual simulator. We created a first-of-a-kind empirical dataset comprising joint kinematics, ground reaction forces, EMG, and joint moments from exoskeletal-assisted and unassisted locomotion. The virtual simulator will provide a low-risk and cost-effective platform

for parametric studies of human-robot interaction during EAL, a necessary step for researchers and clinicians to characterize the effects of human factors on EAL and establish standards for safe and sustained use of robotic exoskeletons. Furthermore, this virtual simulator will provide a platform for exoskeleton companies to conduct rapid design-phase evaluations to accelerate device refinements. We will make all empirical data and virtual simulator code from this study freely available to the research community. We invite investigators to build on our work to develop accurate virtual simulators reproducing EAL to address a broad range of questions, permitting the design and manufacture of exoskeletal devices that more closely replicate a normal gait pattern.

Acknowledgments

We thank Assaf Tzioni from ReWalk Robotics for his support with access to the exoskeleton encoder data. We thank Lina Alsauskaite from ReWalk Robotics for training the research team on safe use of the exoskeleton. ReWalk Robotics did not play any role in study design, participant recruitment, methodology, and data analysis.

Conflict of interest statement

The authors have no conflict of interest to disclose related to this work.

References

1. Mooney LM, Rouse EJ, Herr HM. Autonomous exoskeleton reduces metabolic cost of human walking during load carriage. J Neuroeng Rehabil. 2014;11:80. Epub 2014/06/03. doi: 10.1186/1743-0003-11-80. PubMed PMID: 24885527; PubMed Central PMCID: PMCPMC4036406.

2. Collins SH, Wiggin MB, Sawicki GS. Reducing the energy cost of human walking using an unpowered exoskeleton. Nature. 2015;522(7555):212-5. Epub 2015/04/02. doi: 10.1038/nature14288. PubMed PMID: 25830889; PubMed Central PMCID: PMCPMC4481882.

3. Malcolm P, Galle S, Derave W, De Clercq D. Bi-articular Knee-Ankle-Foot Exoskeleton Produces Higher Metabolic Cost Reduction than Weight-Matched Mono-articular Exoskeleton. Front Neurosci. 2018;12:69. Epub 2018/03/20. doi: 10.3389/fnins.2018.00069. PubMed PMID: 29551959; PubMed Central PMCID: PMCPMC5841020.

4. Fontana M, Vertechy R, Marcheschi S, Salsedo F, Bergamasco M. The body extender: A full-body exoskeleton for the transport and handling of heavy loads. IEEE Robotics and Automation Magazine. 2014;21(4):34-44. doi: 10.1109/MRA.2014.2360287.

5. Wang T, Zhu Y, Zheng T, Sui D, Zhao S, Zhao J. PALExo: A parallel actuated lower limb exoskeleton for high-load carrying. IEEE Access. 2020;8:67250-62. doi: 10.1109/ACCESS.2020.2986357.

6. Thamsuwan O, Milosavljevic S, Srinivasan D, Trask C. Potential exoskeleton uses for reducing low back muscular activity during farm tasks. Am J Ind Med. 2020;63(11):1017-28. Epub 2020/09/15. doi: 10.1002/ajim.23180. PubMed PMID: 32926450.

7. Van Engelhoven L, Poon N, Kazerooni H, Rempel D, Barr A, Harris-Adamson C. Experimental evaluation of a shoulder-support exoskeleton for overhead work: Influences of

496 peak torque amplitude, task, and tool mass. IISE Transactions on Occupational Ergonomics and
497 Human Factors. 2019;7(3-4):250-63. doi: 10.1080/24725838.2019.1637799.
498 8. Tsai CY, Delgado AD, Weinrauch WJ, Manente N, Levy I, Escalon MX, et al.
499 Exoskeletal-assisted walking during acute inpatient rehabilitation leads to motor and functional
500 improvement in persons with spinal cord injury: a pilot study. Arch Phys Med Rehabil.
501 2020;101(4):607-12. Epub 2020/01/01. doi: 10.1016/j.apmr.2019.11.010. PubMed PMID:
502 31891715.
503 9. Hong E, Gorman PH, Forrest GF, Asselin PK, Knezevic S, Scott W, et al. Mobility Skills
504 With Exoskeletal-Assisted Walking in Persons With SCI: Results From a Three Center
505 Randomized Clinical Trial. Frontiers in Robotics and AI. 2020;7(93). doi:
506 10.3389/frobt.2020.00093.
507 10. Ramanujam A, Momeni K, Husain SR, Augustine J, Garbarini E, Barrance P, et al.
508 Mechanisms for improving walking speed after longitudinal powered robotic exoskeleton
509 training for individuals with spinal cord injury. Conf Proc IEEE Eng Med Biol Soc.
510 2018;2018:2805-8. Epub 2018/11/18. doi: 10.1109/EMBC.2018.8512821. PubMed PMID:
511 30440984.
512 11. Asselin PK, Avedissian M, Knezevic S, Kornfeld S, Spungen AM. Training Persons with
513 Spinal Cord Injury to Ambulate Using a Powered Exoskeleton. J Vis Exp. 2016;(112). Epub
514 2016/06/25. doi: 10.3791/54071. PubMed PMID: 27340808; PubMed Central PMCID:
515 PMCPMC4927801.
516 12. Yang A, Asselin P, Knezevic S, Kornfeld S, Spungen AM. Assessment of In-Hospital
517 Walking Velocity and Level of Assistance in a Powered Exoskeleton in Persons with Spinal

Cord Injury. Top Spinal Cord Inj Rehabil. 2015;21(2):100-9. doi: 10.1310/sci2102-100. PubMed PMID: 26364279; PubMed Central PMCID: PMCPMC4568091.

13. Asselin P, Knezevic S, Kornfeld S, Cirnigliaro C, Agranova-Breyter I, Bauman WA, et al. Heart rate and oxygen demand of powered exoskeleton-assisted walking in persons with paraplegia. J Rehabil Res Dev. 2015;52(2):147-58. doi: 10.1682/JRRD.2014.02.0060. PubMed PMID: 26230182.

14. Fineberg DB, Asselin P, Harel NY, Agranova-Breyter I, Kornfeld SD, Bauman WA, et al. Vertical ground reaction force-based analysis of powered exoskeleton-assisted walking in persons with motor-complete paraplegia. J Spinal Cord Med. 2013;36(4):313-21. doi: 10.1179/2045772313Y.0000000126. PubMed PMID: 23820147; PubMed Central PMCID: PMCPMC3758528.

15. Androwis GJ, Sandroff BM, Niewrzol P, Fakhoury F, Wylie GR, Yue G, et al. A pilot randomized controlled trial of robotic exoskeleton-assisted exercise rehabilitation in multiple sclerosis. Mult Scler Relat Disord. 2021;51:102936. Epub 2021/04/21. doi: 10.1016/j.msard.2021.102936. PubMed PMID: 33878619.

16. Karunakaran KK, Gute S, Ames GR, Chervin K, Dandola CM, Nolan KJ. Effect of robotic exoskeleton gait training during acute stroke on functional ambulation. NeuroRehabilitation. 2021. Epub 2021/04/06. doi: 10.3233/NRE-210010. PubMed PMID: 33814476.

17. Ramanujam A, Cirnigliaro CM, Garbarini E, Asselin P, Pilkar R, Forrest GF. Neuromechanical adaptations during a robotic powered exoskeleton assisted walking session. J Spinal Cord Med. 2017:1-11. doi: 10.1080/10790268.2017.1314900. PubMed PMID: 28427305.

18. Kerdraon J, Previnaire JG, Tucker M, Coignard P, Allegre W, Knappen E, et al. Evaluation of safety and performance of the self balancing walking system Atalante in patients with complete motor spinal cord injury. Spinal Cord Ser Cases. 2021;7(1):71. Epub 2021/08/06. doi: 10.1038/s41394-021-00432-3. PubMed PMID: 34349101; PubMed Central PMCID: PMCPMC8338982.

19. Tamburella F, Lorusso M, Tramontano M, Fadlun S, Masciullo M, Scivoletto G. Overground robotic training effects on walking and secondary health conditions in individuals with spinal cord injury: systematic review. J Neuroeng Rehabil. 2022;19(1):27. Epub 2022/03/17. doi: 10.1186/s12984-022-01003-9. PubMed PMID: 35292044.

20. Stampacchia G, Rustici A, Bigazzi S, Gerini A, Tombini T, Mazzoleni S. Walking with a powered robotic exoskeleton: Subjective experience, spasticity and pain in spinal cord injured persons. NeuroRehabilitation. 2016;39(2):277-83. doi: 10.3233/NRE-161358. PubMed PMID: 27372363.

21. Baunsgaard CB, Nissen UV, Brust AK, Frotzler A, Ribeill C, Kalke YB, et al. Exoskeleton gait training after spinal cord injury: An exploratory study on secondary health conditions. J Rehabil Med. 2018;50(9):806-13. Epub 2018/09/06. doi: 10.2340/16501977-2372. PubMed PMID: 30183055.

22. Juszczak M, Gallo E, Bushnik T. Examining the Effects of a Powered Exoskeleton on Quality of Life and Secondary Impairments in People Living With Spinal Cord Injury. Top Spinal Cord Inj Rehabil. 2018;24(4):336-42. Epub 2018/11/22. doi: 10.1310/sci17-00055. PubMed PMID: 30459496; PubMed Central PMCID: PMCPMC6241230.

23. Evans N, Hartigan C, Kandilakis C, Pharo E, Clesson I. Acute Cardiorespiratory and Metabolic Responses During Exoskeleton-Assisted Walking Overground Among Persons with

563 Chronic Spinal Cord Injury. Top Spinal Cord Inj Rehabil. 2015;21(2):122-32. Epub 2015/09/14.
564 doi: 10.1310/sci2102-122. PubMed PMID: 26364281; PubMed Central PMCID:
565 PMCPMC4568093.
566 24. Sale P, Russo EF, Scarton A, Calabro RS, Masiero S, Filoni S. Training for mobility with
567 exoskeleton robot in spinal cord injury patients: a pilot study. Eur J Phys Rehabil Med.
568 2018;54(5):745-51. Epub 2018/03/09. doi: 10.23736/S1973-9087.18.04819-0. PubMed PMID:
569 29517187.
570 25. Kim S, Srinivasan D, Nussbaum MA, Leonessa A. Human gait during level walking with
571 an occupational whole-body powered exoskeleton: not yet a walk in the park. IEEE Access.
572 2021;9:47901-11.
573 26. Talaty M, Esquenazi A, Briceno JE, editors. Differentiating ability in users of the
574 ReWalk TM powered exoskeleton: An analysis of walking kinematics. 2013 IEEE 13th
575 international conference on rehabilitation robotics (ICORR); 2013: IEEE.
576 27. Ekelem A, Goldfarb M. Supplemental Stimulation Improves Swing Phase Kinematics
577 During Exoskeleton Assisted Gait of SCI Subjects With Severe Muscle Spasticity. Front
578 Neurosci. 2018;12:374. Epub 2018/06/19. doi: 10.3389/fnins.2018.00374. PubMed PMID:
579 29910710; PubMed Central PMCID: PMCPMC5992413.
580 28. Chang SH, Zhu F, Patel N, Afzal T, Kern M, Francisco GE. Combining robotic
581 exoskeleton and body weight unweighing technology to promote walking activity in tetraplegia
582 following SCI: A case study. J Spinal Cord Med. 2020;43(1):126-9. Epub 2018/10/20. doi:
583 10.1080/10790268.2018.1527078. PubMed PMID: 30335593; PubMed Central PMCID:
584 PMCPMC7006789.

585 29. Bellitto A, Mandraccia S, Leoncini C, Rossi L, Gamba S, Massone A, et al., editors.
586 Walking after incomplete spinal cord injury: changes in muscle activations due to training with a
587 robotic powered exoskeleton. 2020 8th IEEE RAS/EMBS International Conference for
588 Biomedical Robotics and Biomechatronics (BioRob); 2020; New York City, NY: IEEE.
589 30. Escalona MJ, Bourbonnais D, Goyette M, Duclos C, Gagnon DH. Wearable exoskeleton
590 control modes selected during overground walking affect muscle synergies in adults with a
591 chronic incomplete spinal cord injury. Spinal Cord Ser Cases. 2020;6(1):26. Epub 2020/04/26.
592 doi: 10.1038/s41394-020-0269-6. PubMed PMID: 32332703; PubMed Central PMCID:
593 PMCPMC7182571.
594 31. Safavi S, Ghafari AS, Meghdari A, editors. Design of an optimum torque actuator for
595 augmenting lower extremity exoskeletons in biomechanical framework. IEEE International
596 Conference on Robotics and Biomimetics; 2011; Phuket, Thailand.
597 32. Guan X, Ji L, Wang R, Huang W, editors. Optimization of an unpowered energy-stored
598 exoskeleton for patients with spinal cord injury. 38th Annual International Conference of the
599 IEEE Engineering in Medicine and Biology Society; 2016; Orlando, FL.
600 33. Hegarty AK, Petrella AJ, Kurz MJ, Silverman AK. Evaluating the Effects of Ankle-Foot
601 Orthosis Mechanical Property Assumptions on Gait Simulation Muscle Force Results. J Biomech
602 Eng. 2017;139(3). Epub 2016/12/18. doi: 10.1115/1.4035472. PubMed PMID: 27987301.
603 34. Arch ES, Stanhope SJ, Higginson JS. Passive-dynamic ankle-foot orthosis replicates
604 soleus but not gastrocnemius muscle function during stance in gait: Insights for orthosis
605 prescription. Prosthet Orthot Int. 2016;40(5):606-16. Epub 2015/07/26. doi:
606 10.1177/0309364615592693. PubMed PMID: 26209424.

35. Manns P, Sreenivasa M, Millard M, Mombaur K. Motion optimization and parameter identification for a human and lower back exoskeleton model. IEEE Robotics and Automation Letters. 2017;2(3):1564-70.

36. Cseke B, Uchida T, Doumit M. Simulating Ideal Assistive Strategies to Reduce the Metabolic Cost of Walking in the Elderly. IEEE Trans Biomed Eng. 2022;PP. Epub 2022/02/25. doi: 10.1109/TBME.2022.3153951. PubMed PMID: 35201978.

37. Bianco NA, Franks PW, Hicks JL, Delp SL. Coupled exoskeleton assistance simplifies control and maintains metabolic benefits: A simulation study. PLoS One. 2022;17(1):e0261318. Epub 2022/01/06. doi: 10.1371/journal.pone.0261318. PubMed PMID: 34986191; PubMed Central PMCID: PMCPMC8730392.

38. Franks PW, Bianco NA, Bryan GM, Hicks JL, Delp SL, Collins SH, editors. Testing simulated assistance strategies on a hip-knee-ankle exoskeleton: a case study. 8th IEEE RAS/EMBS International Conference for Biomedical Robotics and Biomechatronics (BioRob); 2020; New York: IEEE.

39. Durandau G, Farina D, Asin-Prieto G, Dimbwadyo-Terrer I, Lerma-Lara S, Pons JL, et al. Voluntary control of wearable robotic exoskeletons by patients with paresis via neuromechanical modeling. J Neuroeng Rehabil. 2019;16(1):91. Epub 2019/07/19. doi: 10.1186/s12984-019-0559-z. PubMed PMID: 31315633; PubMed Central PMCID: PMCPMC6637518.

40. Dembia CL, Silder A, Uchida TK, Hicks JL, Delp SL. Simulating ideal assistive devices to reduce the metabolic cost of walking with heavy loads. PLoS One. 2017;12(7):e0180320. Epub 2017/07/13. doi: 10.1371/journal.pone.0180320. PubMed PMID: 28700630; PubMed Central PMCID: PMCPMC5507502.

630 41. Uchida TK, Seth A, Pouya S, Dembia CL, Hicks JL, Delp SL. Simulating Ideal Assistive
631 Devices to Reduce the Metabolic Cost of Running. PLoS One. 2016;11(9):e0163417. Epub
632 2016/09/23. doi: 10.1371/journal.pone.0163417. PubMed PMID: 27656901; PubMed Central
633 PMCID: PMCPMC5033584.
634 42. Nguyen VQ, Umberger BR, Sup FC. Predictive Simulation of Human Walking
635 Augmented by a Powered Ankle Exoskeleton. IEEE Int Conf Rehabil Robot; Jun2019. p. 53-8.
636 43. Lim B, Hyoung S, Lee J, Seo K, Jang J, Shim Y, editors. Simulating gait assistance of a
637 hip exoskeleton: case studies for ankle pathologies. 2017 IEEE International Conference on
638 Robotics and Automation; 2017.
639 44. Lerner ZF, Damiano DL, Bulea TC. Computational modeling of neuromuscular response
640 to swing-phase robotic knee extension assistance in cerebral palsy. J Biomech. 2019;87:142-9.
641 Epub 2019/03/14. doi: 10.1016/j.jbiomech.2019.02.025. PubMed PMID: 30862380; PubMed
642 Central PMCID: PMCPMC6534383.
643 45. Cho K, Kim Y, Yi D, Jung M, Lee K. Analysis and evaluation of a combined human –
644 exoskeleton model under two different constraints condition. International Summit on Human
645 Simulation 2012; May 20-22; St. Pete Beach, FL2012.
646 46. Ferrati F, Bortoletto R, Pagello E. Virtual Modelling of a Real Exoskeleton Constrained
647 to a Human Musculoskeletal Model. Biomimetic and Biohybrid Systems. Berlin, Heidelberg:
648 Springer; 2013. p. 96-107.
649 47. Fournier BN, Lemaire ED, Smith AJJ, Doumit M. Modeling and Simulation of a Lower
650 Extremity Powered Exoskeleton. IEEE transactions on neural systems and rehabilitation
651 engineering : a publication of the IEEE Engineering in Medicine and Biology Society.

652 2018;26(8):1596-603. Epub 2018/07/14. doi: 10.1109/TNSRE.2018.2854605. PubMed PMID:
653 30004879.
654 48. Zhu Y, Zhang G, Zhang C, Liu G, Zhao J. Biomechanical modeling and load-carrying
655 simulation of lower limb exoskeleton. Biomed Mater Eng. 2015;26 Suppl 1:S729-38. Epub
656 2015/09/26. doi: 10.3233/BME-151364. PubMed PMID: 26406068.
657 49. Torricelli D, Cortés C, Lete N, Bertelsen Á, Gonzalez-Vargas JE, del-Ama AJ, et al. A
658 Subject-Specific Kinematic Model to Predict Human Motion in Exoskeleton-Assisted Gait.
659 Frontiers in Neurorobotics. 2018;12(18). doi: 10.3389/fnbot.2018.00018.
660 50. Khamar M, Edrisi M, Zahiri M. Human-exoskeleton control simulation, kinetic and
661 kinematic modeling and parameters extraction. MethodsX. 2019;6:1838-46. Epub 2019/09/12.
662 doi: 10.1016/j.mex.2019.08.014. PubMed PMID: 31508321; PubMed Central PMCID:
663 PMCPMC6726754.
664 51. ReWalk. ReWalk 6.0 Personal System User Guide. ReWalk Robotics. 2020:1-97.
665 52. Leboeuf F, Baker R, Barre A, Reay J, Jones R, Sangeux M. The conventional gait model,
666 an open-source implementation that reproduces the past but prepares for the future. Gait Posture.
667 2019;69:235-41. Epub 2019/04/28. doi: 10.1016/j.gaitpost.2019.04.015. PubMed PMID:
668 31027876.
669 53. Rajagopal A, Dembia CL, DeMers MS, Delp DD, Hicks JL, Delp SL. Full-Body
670 Musculoskeletal Model for Muscle-Driven Simulation of Human Gait. IEEE Trans Biomed Eng.
671 2016;63(10):2068-79. Epub 2016/07/09. doi: 10.1109/TBME.2016.2586891. PubMed PMID:
672 27392337; PubMed Central PMCID: PMCPMC5507211.
673 54. Rutherford DJ, Hubley-Kozey CL, Stanish WD. Maximal voluntary isometric contraction
674 exercises: a methodological investigation in moderate knee osteoarthritis. J Electromyogr

675 Kinesiol. 2011;21(1):154-60. Epub 2010/10/12. doi: 10.1016/j.jelekin.2010.09.004. PubMed
676 PMID: 20926310.
677 55. Perotto A, Delagi EF, Iazzetti J, Morrison D. Anatomical Guide for the
678 Electromyographer. 4th ed. Springfield, IL: Charles C. Thomas; 2005. 345 p.
679 56. Pal S, Draper CE, Fredericson M, Gold GE, Delp SL, Beaupre GS, et al. Patellar
680 maltracking correlates with vastus medialis activation delay in patellofemoral pain patients. Am
681 J Sports Med. 2011;39(3):590-8. Epub 2010/11/16. doi: 10.1177/0363546510384233. PubMed
682 PMID: 21076015.
683 57. Delp SL, Anderson FC, Arnold AS, Loan P, Habib A, John CT, et al. OpenSim: open-
684 source software to create and analyze dynamic simulations of movement. IEEE transactions on
685 biomedical engineering. 2007;54(11):1940-50.
686 58. Thelen DG, Anderson FC, Delp SL. Generating dynamic simulations of movement using
687 computed muscle control. J Biomech. 2003;36(3):321-8. doi: SP-113. PubMed PMID:
688 12594980.
689 59. Delp SL, Loan JP, Hoy MG, Zajac FE, Topp EL, Rosen JM. An interactive graphics-
690 based model of the lower extremity to study orthopaedic surgical procedures. IEEE Trans
691 Biomed Eng. 1990;37(8):757-67. doi: SP-24/JL-439. PubMed PMID: 2210784.
692 60. Delp SL, Anderson FC, Arnold AS, Loan P, Habib A, John CT, et al. OpenSim: open-
693 source software to create and analyze dynamic simulations of movement. IEEE Trans Biomed
694 Eng. 2007;54(11):1940-50. Epub 2007/11/21. doi: 10.1109/TBME.2007.901024. PubMed
695 PMID: 18018689.
696 61. Grabke EP, Masani K, Andrysek J. Lower Limb Assistive Device Design Optimization
697 Using Musculoskeletal Modeling: A Review. ASME J Med Devices. 2019;13(4).

62. Sartori M, Durandau G, Farina D, editors. Neuromusculoskeletal models of human-machine interaction in individuals wearing lower limb assistive technologies. Third International Conference on NeuroRehabilitation; 2017; Segovia, Spain.

63. Dixon PC, Jansen K, Jonkers I, Stebbins J, Theologis T, Zavatsky AB. Muscle contributions to centre of mass acceleration during turning gait in typically developing children: A simulation study. J Biomech. 2015;48(16):4238-45. Epub 2015/11/12. doi: 10.1016/j.jbiomech.2015.10.028. PubMed PMID: 26555714.

64. Jackson RW, Dembia CL, Delp SL, Collins SH. Muscle-tendon mechanics explain unexpected effects of exoskeleton assistance on metabolic rate during walking. J Exp Biol. 2017;220(Pt 11):2082-95. Epub 2017/03/28. doi: 10.1242/jeb.150011. PubMed PMID: 28341663.

Supporting information

S1 Fig. Average (±1 SD) joint angles from four exoskeletal-assited (A-F; human: blue for left leg, red for right leg; robot: black) and five unassisted (G-L; human: blue for left leg, red for right leg) sit-to-stand trials. The offset in angles between the human (blue or red) and the robot (black) was due to different definitions of coordinate axes for each rigid body. (A-F) The first dashed vertical lines represent the transition from positioning phase (user gets in to position by flexing the torso forward and loading the crutches) to hold phase (leaned forward for 3 seconds). The second dashed vertical lines represent the beginning of the rise phase, with the hip and knee motors activating to complete the sit-to-stand maneuver.

S2 Fig. Average (±1 SD) ground reaction forces from four exoskeletal-assited (A-C) and five unassisted (D-F) sit-to-stand trials. The ground reaction forces from exoskeletal-assisted locomotion were normalized to the combined weight of the participant and the exoskeleton; forces from unassisted locomotion were normalized to the participant's body weight (BW). (A-C) The first dashed vertical lines represent the transition from positioning phase (user gets in to position by flexing the torso forward and loading the crutches) to hold phase (leaned forward for 3 seconds). The second dashed vertical lines represent the beginning of the rise phase, with the hip and knee motors activating to complete the sit-to-stand maneuver. A-P = Anterior-Posterior, M-L = Medial-Lateral.

S3 Fig. Average (+1 SD) normalized electromyography (EMG) data from four exoskeletal-assisted (A-H) and five unassisted (I-P) sit-to-stand trials. The EMG data were normalized using muscle-specific maximum voluntary contraction values. (A-H) The first dashed vertical lines represent the transition from positioning phase (user gets in to position by flexing the torso forward and loading the crutches) to hold phase (leaned forward for 3 seconds). The second

735 dashed vertical lines represent the beginning of the rise phase, with the hip and knee motors
736 activating to complete the sit-to-stand maneuver. RF = rectus femoris, VL = vastus lateralis, VM
737 = vastus medialis, ST = semitendinosus, BF = biceps femoris, GM = gastrocnemius medialis,
738 SOL = soleus, TIB = tibialis anterior.

739 **S4 Fig.** Average (±1 SD) joint moments from four exoskeletal-assited (A-F) and five unassisted
740 (G-L) sit-to-stand trials. The joint moments from exoskeletal-assisted locomotion were
741 normalized to the combined mass of the participant and the exoskeleton; joint moments from
742 unassisted locomotion were normalized to the participant's mass. (A-F) The first dashed vertical
743 lines represent the transition from positioning phase (user gets in to position by flexing the torso
744 forward and loading the crutches) to hold phase (leaned forward for 3 seconds). The second
745 dashed vertical lines represent the beginning of the rise phase, with the hip and knee motors
746 activating to complete the sit-to-stand maneuver.

747 **S5 Fig.** Average (±1 SD) joint angles from five exoskeletal-assited (A-F; human: blue for left
748 leg, red for right leg; robot: black) and five unassisted (G-L; human: blue for left leg, red for
749 right leg) stand-to-sit trials. The offset in angles between the human (blue or red) and the robot
750 (black) was due to different definitions of coordinate axes for each rigid body. (A-F) The first
751 dashed vertical lines represent the transition from positioning phase (user gets in to position by
752 leaning backwards and loading the crutches) to hold phase (leaned backward for 3 seconds). The
753 second dashed vertical lines represent the beginning of the descend phase, with the hip and knee
754 motors activating to complete the stand-to-sit maneuver.

755 **S6 Fig.** Average (±1 SD) ground reaction forces from five exoskeletal-assited (A-C) and five
756 unassisted (D-F) stand-to-sit trials. The ground reaction forces from exoskeletal-assisted
757 locomotion were normalized to the combined weight of the participant and the exoskeleton;

forces from unassisted locomotion were normalized to the participant's body weight (BW). (A-C) The first dashed vertical lines represent the transition from positioning phase (user gets in to position by leaning backwards and loading the crutches) to hold phase (leaned backward for 3 seconds). The second dashed vertical lines represent the beginning of the descend phase, with the hip and knee motors activating to complete the stand-to-sit maneuver. A-P = Anterior-Posterior, M-L = Medial-Lateral.

S7 Fig. Average (+1 SD) normalized electromyography (EMG) data from five exoskeletal-assisted (A-H) and five unassisted (I-P) stand-to-sit trials. The EMG data were normalized using muscle-specific maximum voluntary contraction values. (A-H) The first dashed vertical lines represent the transition from positioning phase (user gets in to position by leaning backwards and loading the crutches) to hold phase (leaned backward for 3 seconds). The second dashed vertical lines represent the beginning of the descend phase, with the hip and knee motors activating to complete the stand-to-sit maneuver. RF = rectus femoris, VL = vastus lateralis, VM = vastus medialis, ST = semitendinosus, BF = biceps femoris, GM = gastrocnemius medialis, SOL = soleus, TIB = tibialis anterior.

S8 Fig. Average (±1 SD) joint moments from five exoskeletal-assited (A-F) and five unassisted (G-L) stand-to-sit trials. The joint moments from exoskeletal-assisted locomotion were normalized to the combined mass of the participant and the exoskeleton; joint moments from unassisted locomotion were normalized to the participant's mass. (A-F) The first dashed vertical lines represent the transition from positioning phase (user gets in to position by leaning backwards and loading the crutches) to hold phase (leaned backward for 3 seconds). The second dashed vertical lines represent the beginning of the descend phase, with the hip and knee motors activating to complete the stand-to-sit maneuver.

(A) Marker set (front)

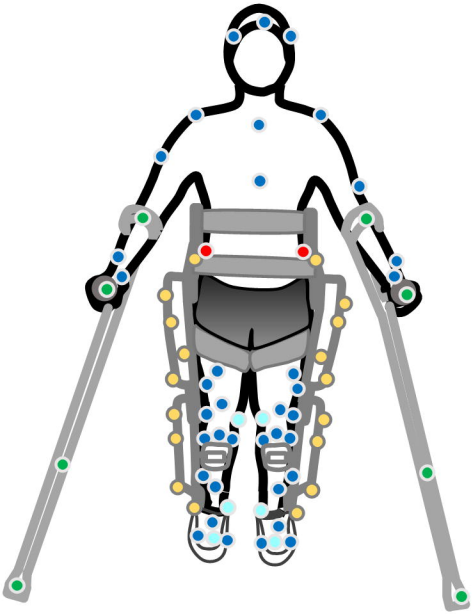

(B) Marker set (back)

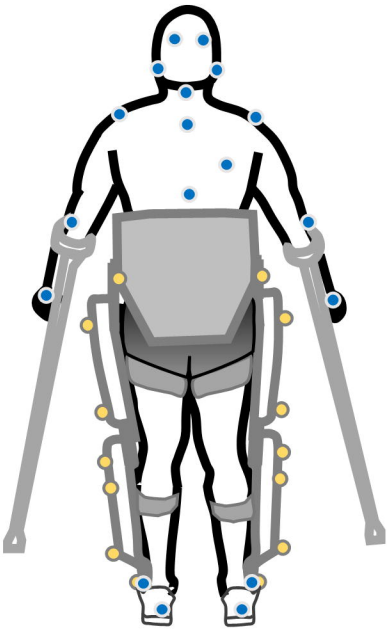

(C) Human-Robot Joints

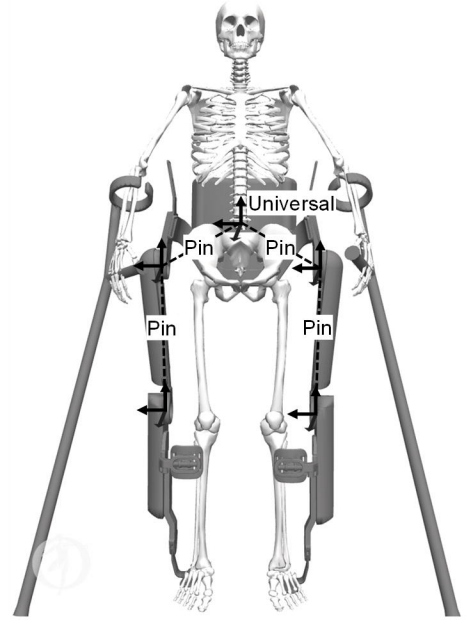

(D) Subject-specific model

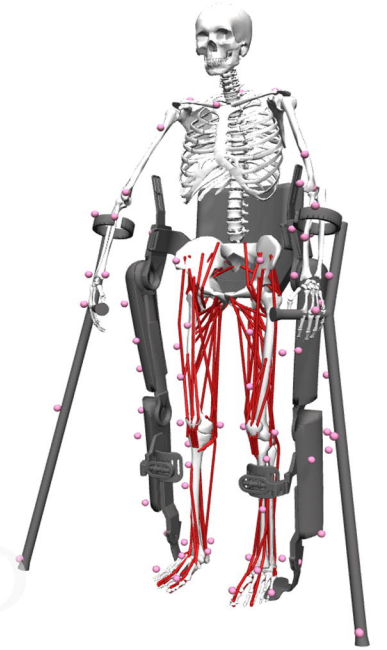

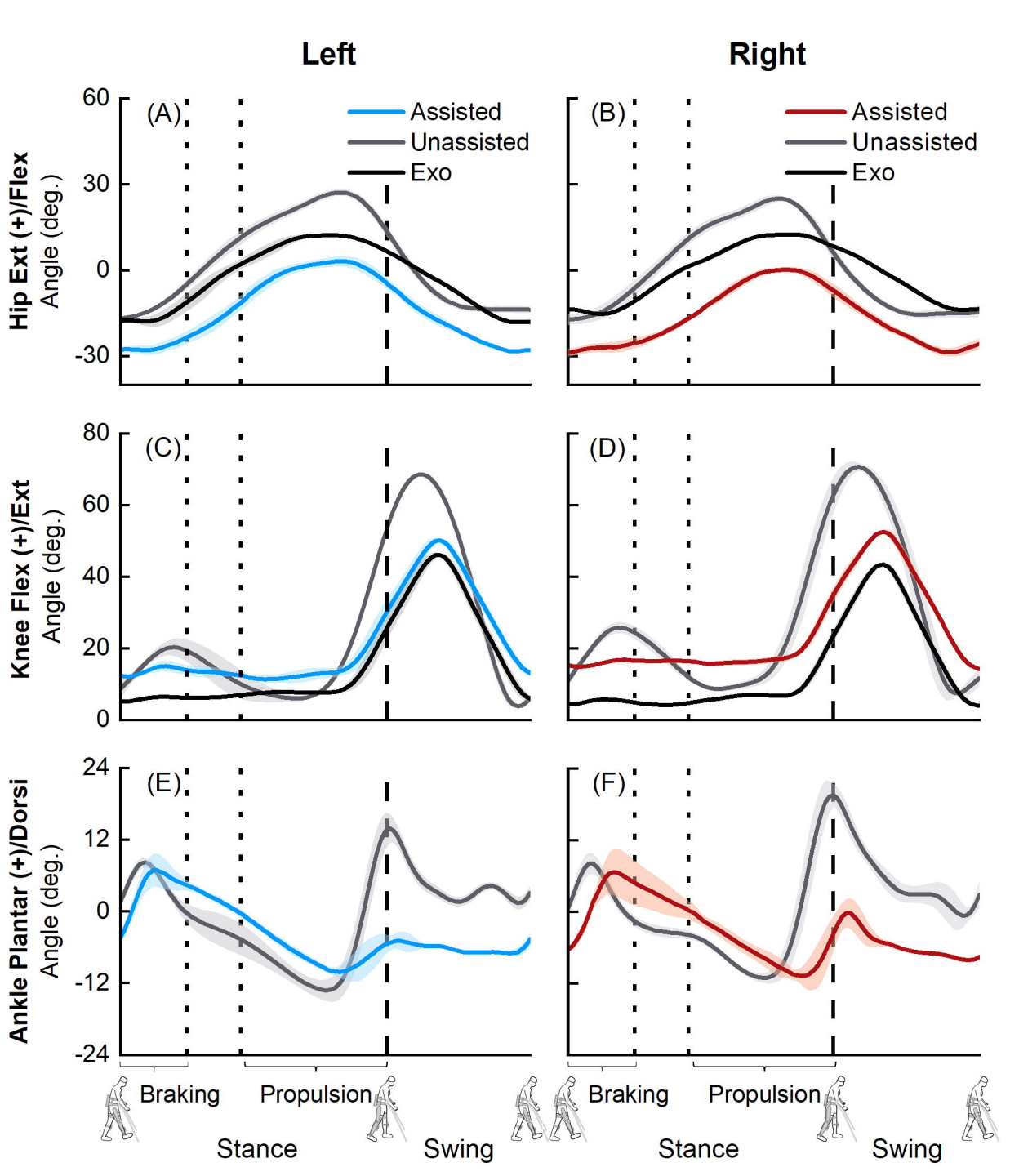
Left
Right
(A)
(B)
(C)
(D)
(E)
(F)
Assisted
Unassisted
Exo
Hip Ext (+)/Flex
Angle (deg.)
Knee Flex (+)/Ext
Angle (deg.)
Ankle Plantar (+)/Dorsi
Angle (deg.)
60
30
0
-30
80
60
40
20
0
24
12
0
-12
-24
Braking
Propulsion
Stance
Swing

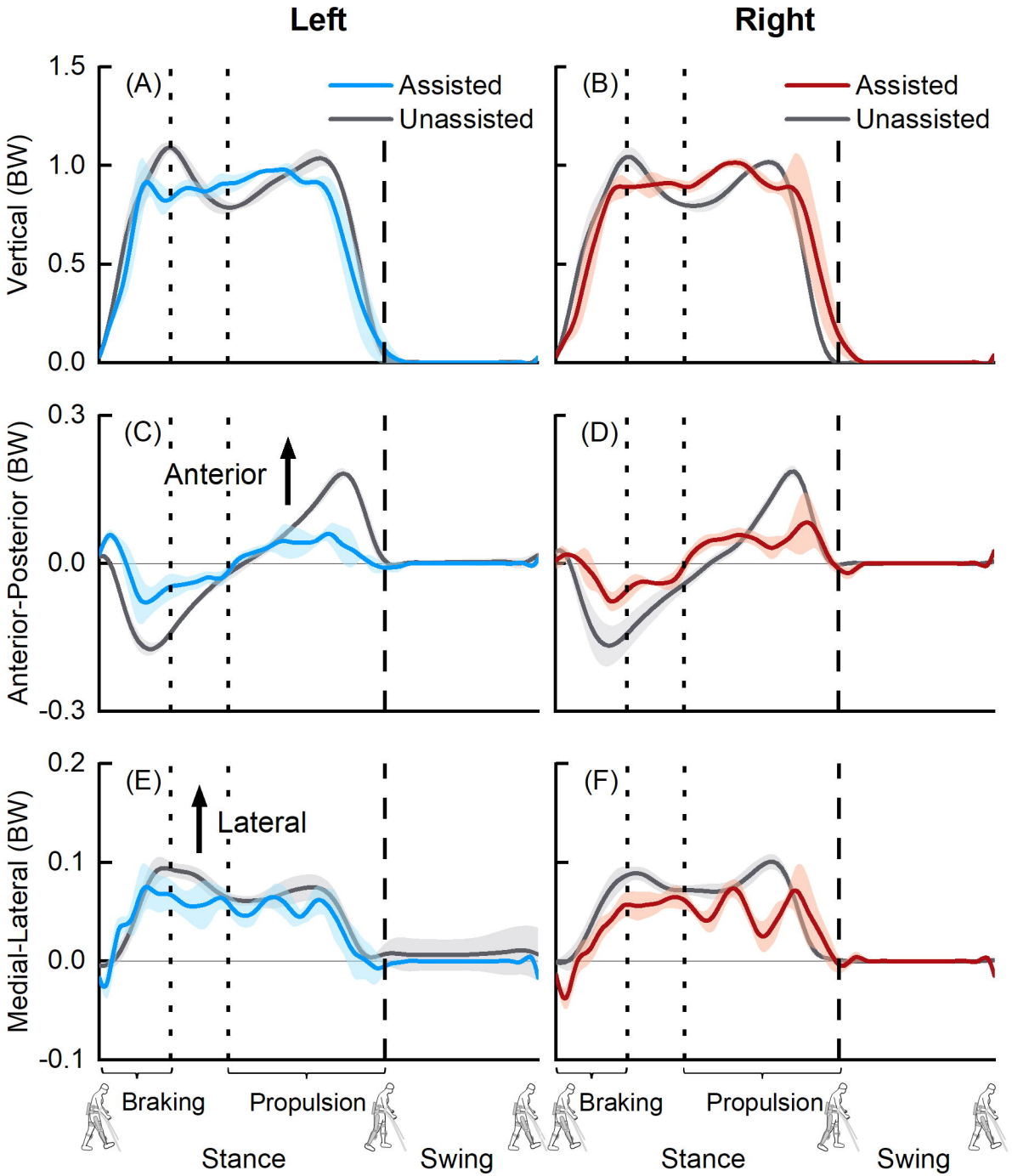
Left
Right
(A)
(B)
Assisted
Unassisted
Vertical (BW)
1.5
1.0
0.5
0.0
(C)
(D)
Anterior
Anterior-Posterior (BW)
0.3
0.0
-0.3
(E)
(F)
Lateral
Medial-Lateral (BW)
0.2
0.1
0.0
-0.1
Braking
Propulsion
Stance
Swing

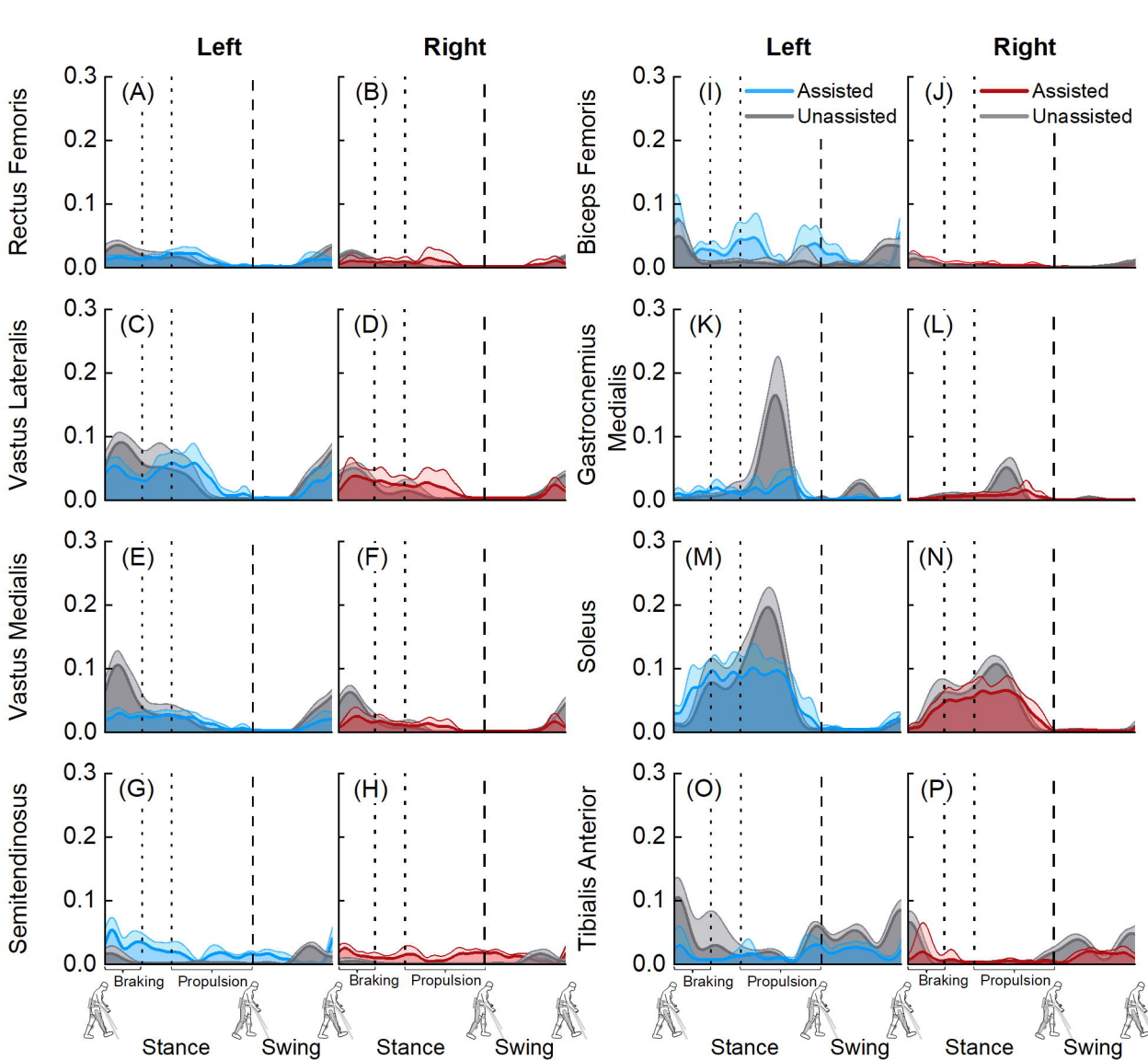
Left
Right
Left
Right
Rectus Femoris
Biceps Femoris
Vastus Lateralis
Gastrocnemius Medialis
Vastus Medialis
Soleus
Semitendinosus
Tibialis Anterior
(A)
(B)
(C)
(D)
(E)
(F)
(G)
(H)
(I)
(J)
(K)
(L)
(M)
(N)
(O)
(P)
Assisted
Unassisted
Assisted
Unassisted
0.3
0.2
0.1
0.0
Braking
Propulsion
Stance
Swing
Stance
Swing
Braking
Propulsion
Stance
Swing
Stance
Swing

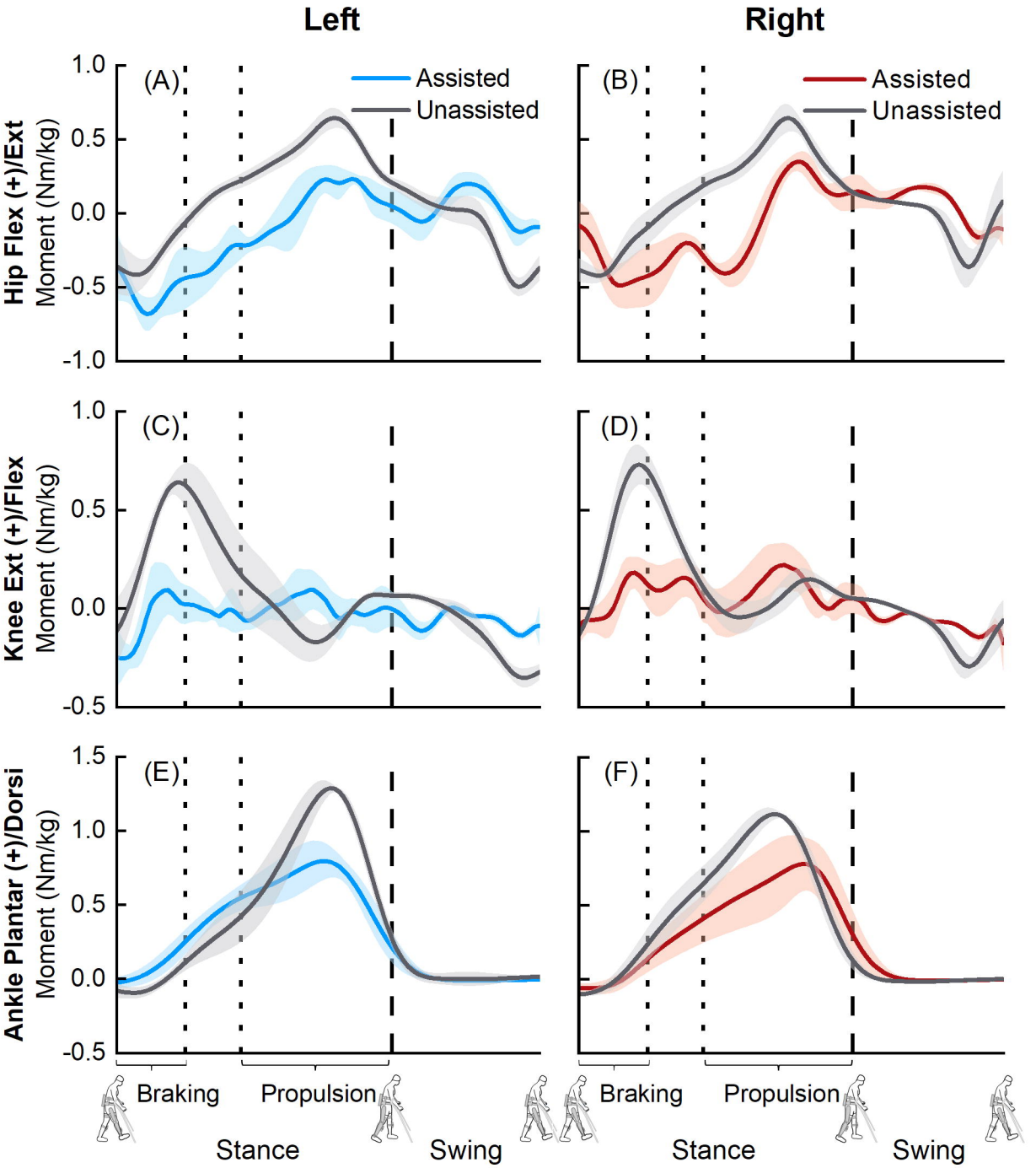
Left
Right
(A)
(B)
(C)
(D)
(E)
(F)
Assisted
Unassisted
Hip Flex (+)/Ext
Moment (Nm/kg)
Knee Ext (+)/Flex
Moment (Nm/kg)
Ankle Plantar (+)/Dorsi
Moment (Nm/kg)
1.0
0.5
0.0
-0.5
-1.0
1.5
Braking
Propulsion
Stance
Swing

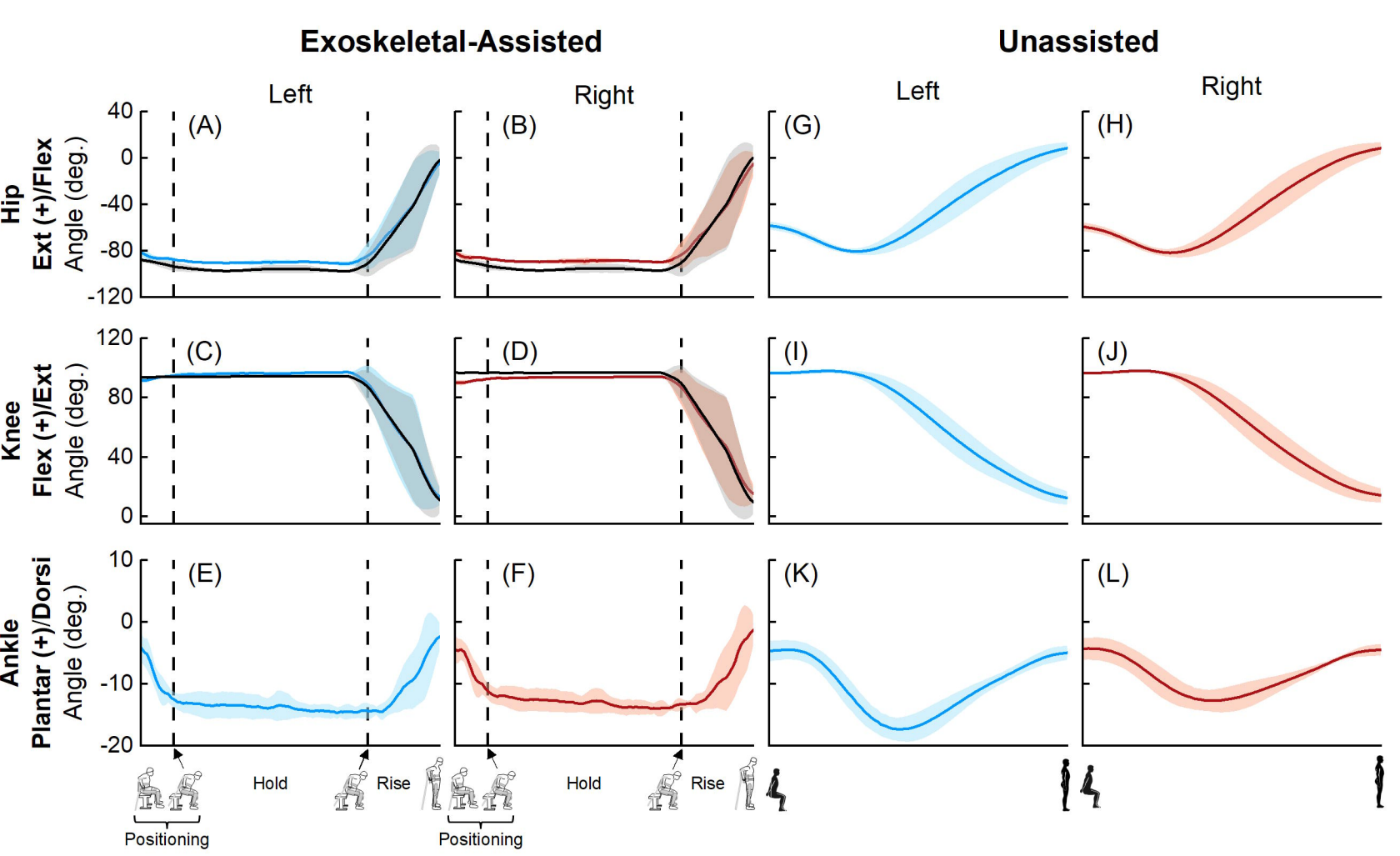
Exoskeletal-Assisted
Unassisted
Left
Right
Left
Right
Hip
Ext (+)/Flex
Angle (deg.)
40
0
-40
-80
-120
(A)
(B)
(G)
(H)
Knee
Flex (+)/Ext
Angle (deg.)
120
80
40
0
(C)
(D)
(I)
(J)
Ankle
Plantar (+)/Dorsi
Angle (deg.)
10
0
-10
-20
(E)
(F)
(K)
(L)
Positioning
Hold
Rise
Positioning
Hold
Rise

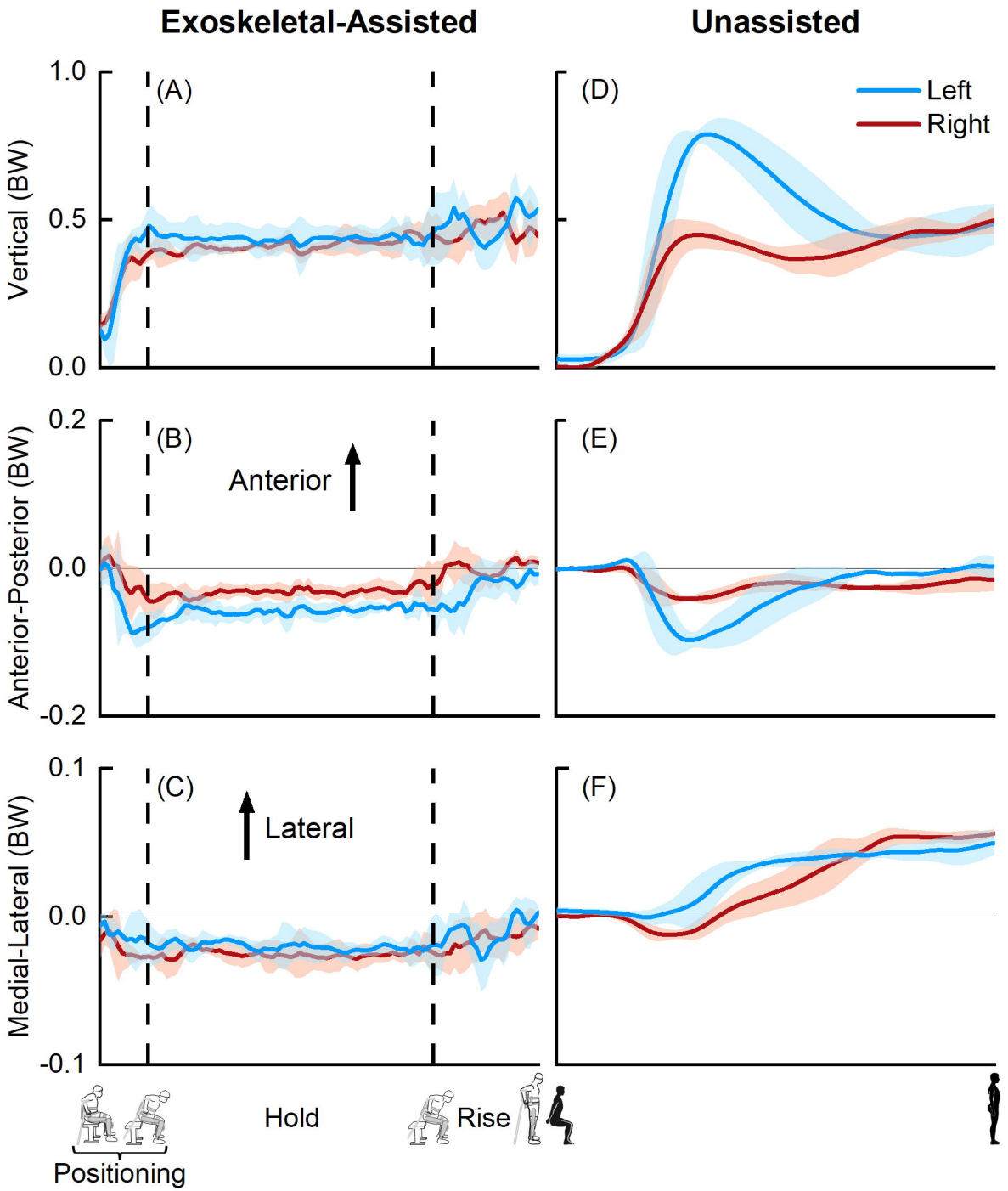
Exoskeletal-Assisted
Unassisted
(A)
(B)
(C)
(D)
(E)
(F)
Left
Right
Vertical (BW)
Anterior-Posterior (BW)
Medial-Lateral (BW)
1.0
0.5
0.0
0.2
0.0
-0.2
0.1
0.0
-0.1
Anterior
Lateral
Positioning
Hold
Rise

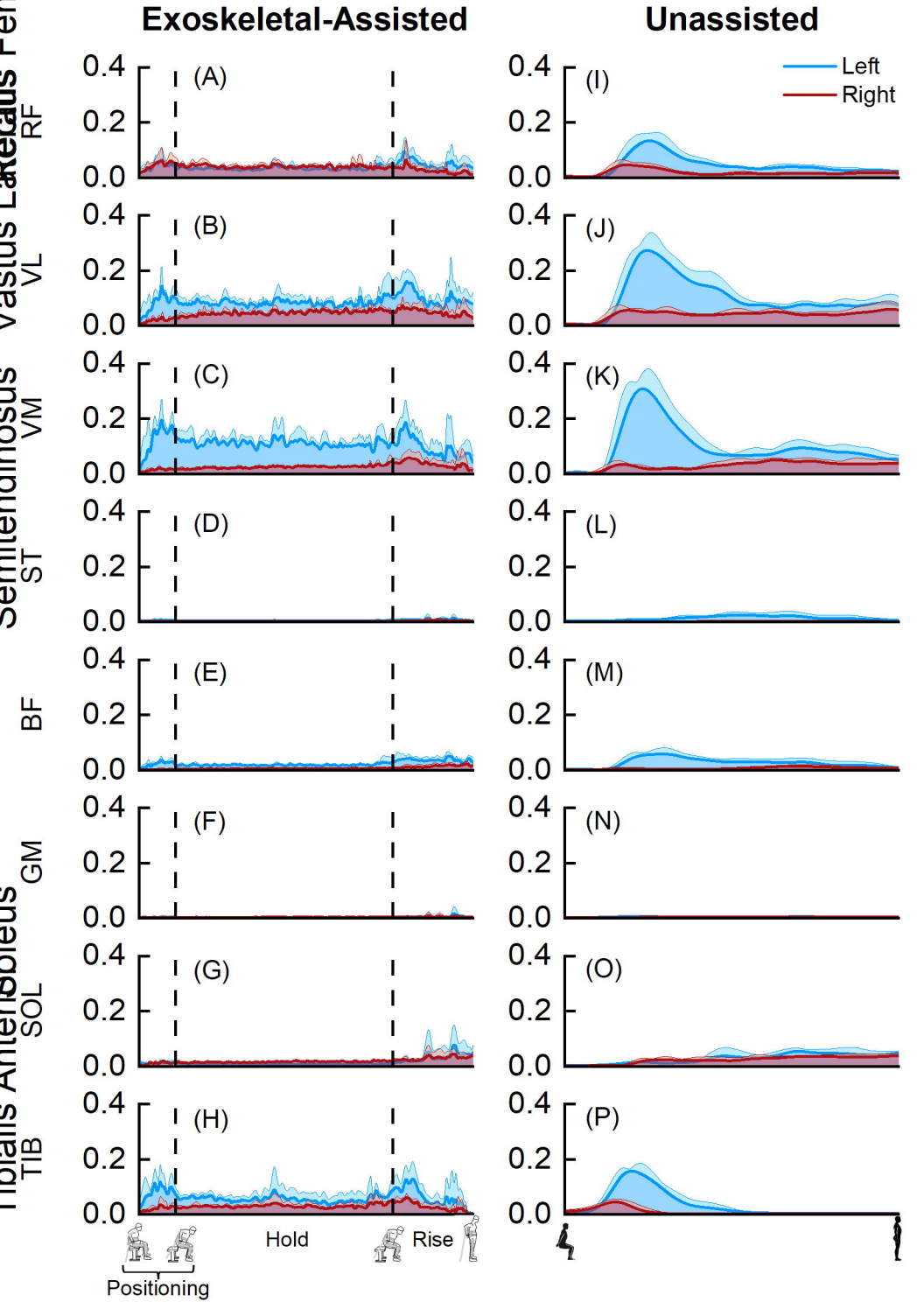
Exoskeletal-Assisted
Unassisted
Left
Right
(A)
(B)
(C)
(D)
(E)
(F)
(G)
(H)
(I)
(J)
(K)
(L)
(M)
(N)
(O)
(P)
RF
VL
VM
ST
BF
GM
SOL
TIB
0.4
0.2
0.0
Hold
Rise
Positioning

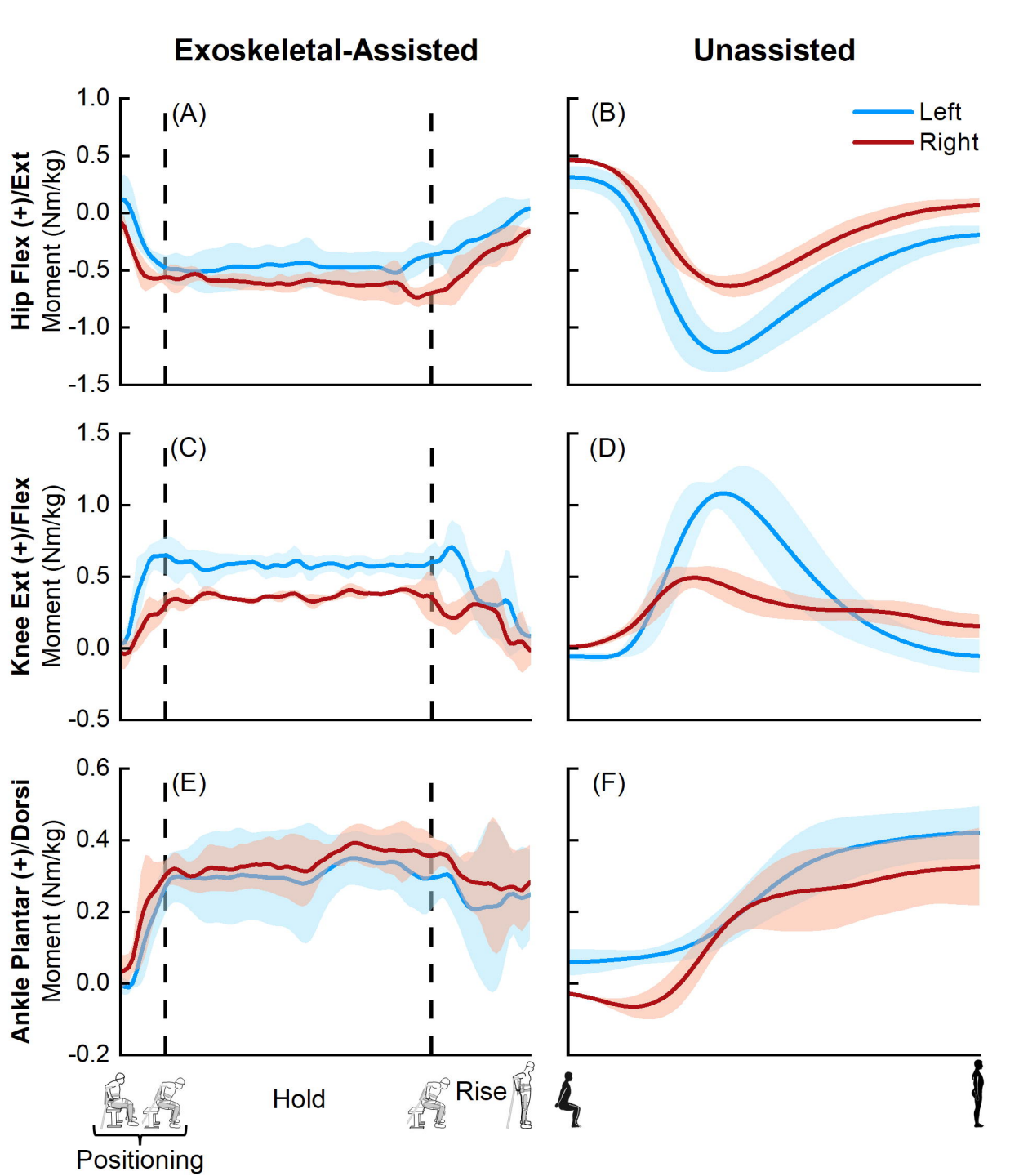
Exoskeletal-Assisted
Unassisted
(A)
(B)
(C)
(D)
(E)
(F)
Left
Right
Hip Flex (+)/Ext
Moment (Nm/kg)
Knee Ext (+)/Flex
Moment (Nm/kg)
Ankle Plantar (+)/Dorsi
Moment (Nm/kg)
1.0
0.5
0.0
-0.5
-1.0
-1.5
1.5
1.0
0.5
0.0
-0.5
0.6
0.4
0.2
0.0
-0.2
Positioning
Hold
Rise

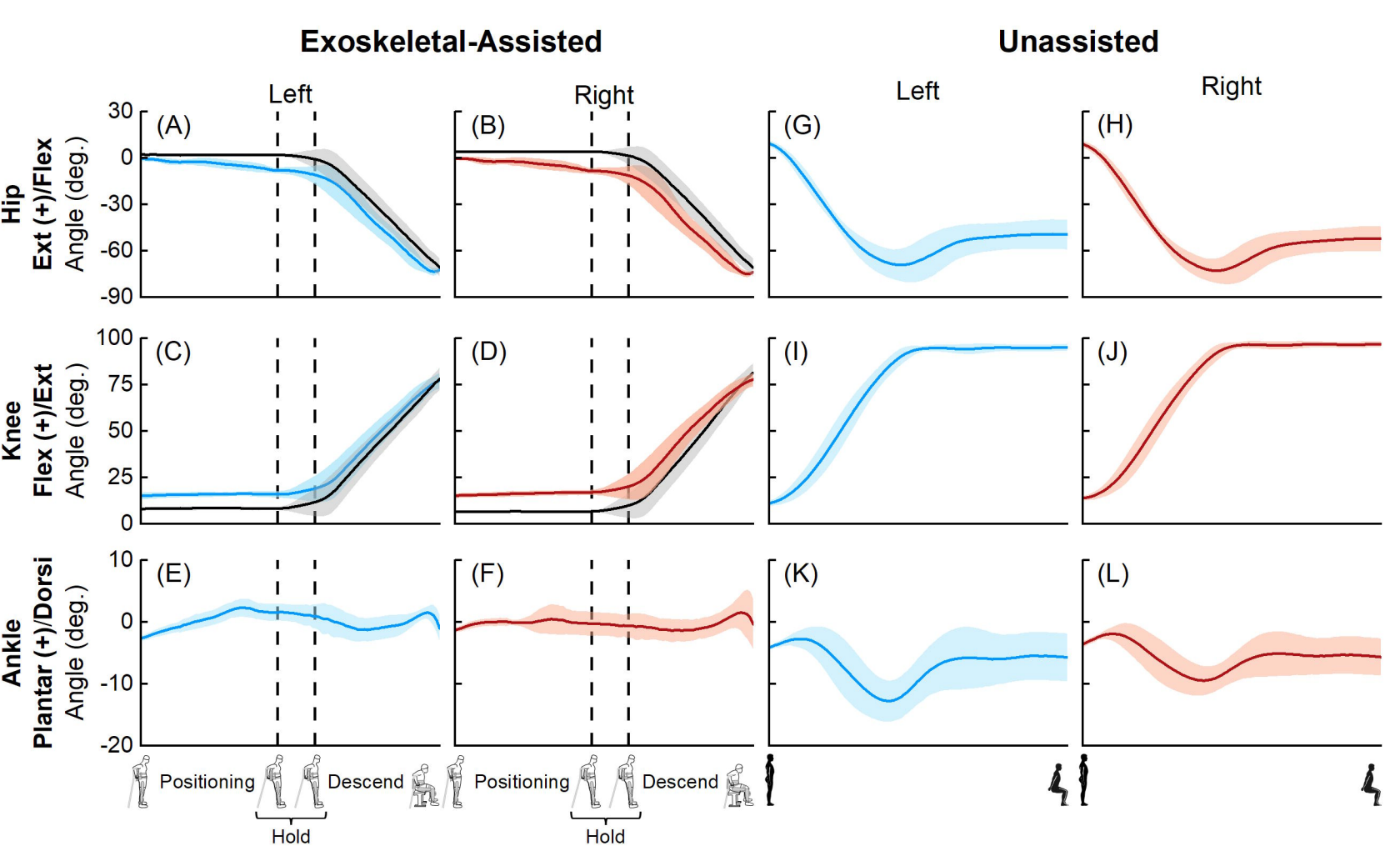
Exoskeletal-Assisted
Unassisted
Left
Right
Left
Right
Hip
Ext (+)/Flex
Angle (deg.)
Knee
Flex (+)/Ext
Angle (deg.)
Ankle
Plantar (+)/Dorsi
Angle (deg.)
30
0
-30
-60
-90
100
75
50
25
0
10
0
-10
-20
(A)
(B)
(C)
(D)
(E)
(F)
(G)
(H)
(I)
(J)
(K)
(L)
Positioning
Descend
Hold
Positioning
Descend
Hold

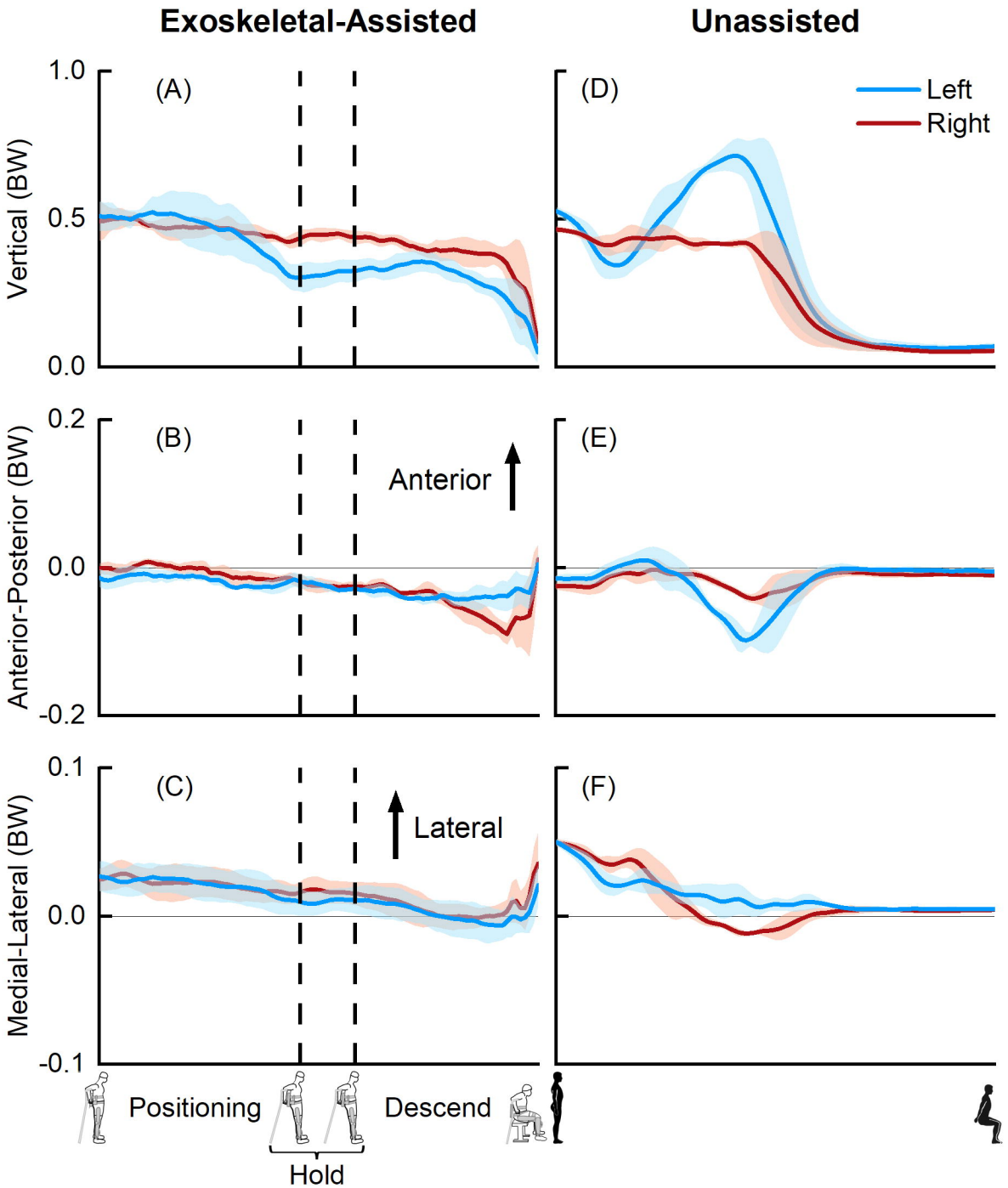
Exoskeletal-Assisted
Unassisted
(A)
(B)
(C)
(D)
(E)
(F)
Left
Right
Vertical (BW)
Anterior-Posterior (BW)
Medial-Lateral (BW)
1.0
0.5
0.0
0.2
0.0
-0.2
0.1
0.0
-0.1
Anterior
Lateral
Positioning
Hold
Descend

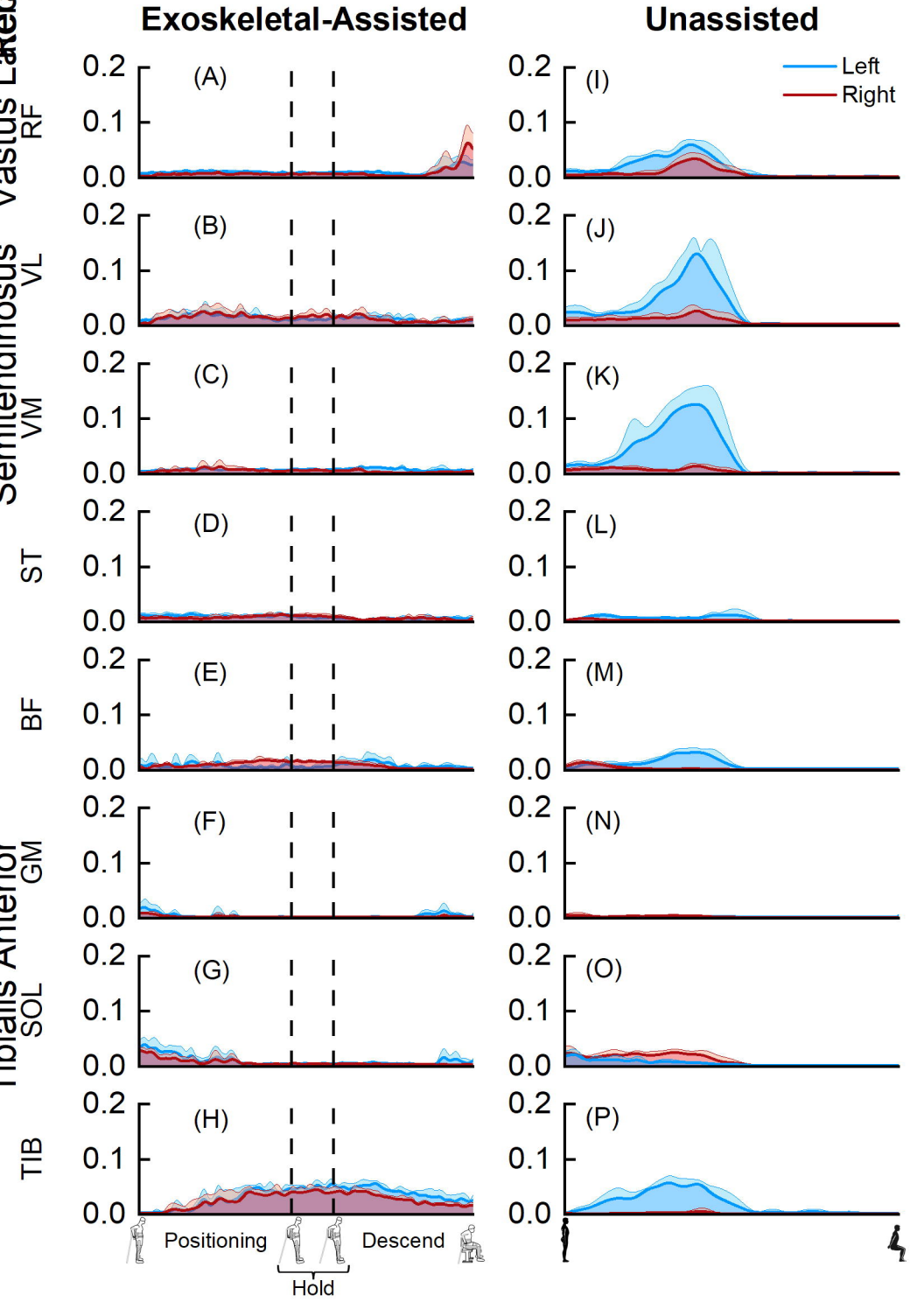
Exoskeletal-Assisted
Unassisted
Left
Right
Vastus Lateralis
RF
Semitendinosus
VL
VM
ST
BF
Tibialis Anterior
GM
SOL
TIB
(A)
(B)
(C)
(D)
(E)
(F)
(G)
(H)
(I)
(J)
(K)
(L)
(M)
(N)
(O)
(P)
0.2
0.1
0.0
Positioning
Hold
Descend

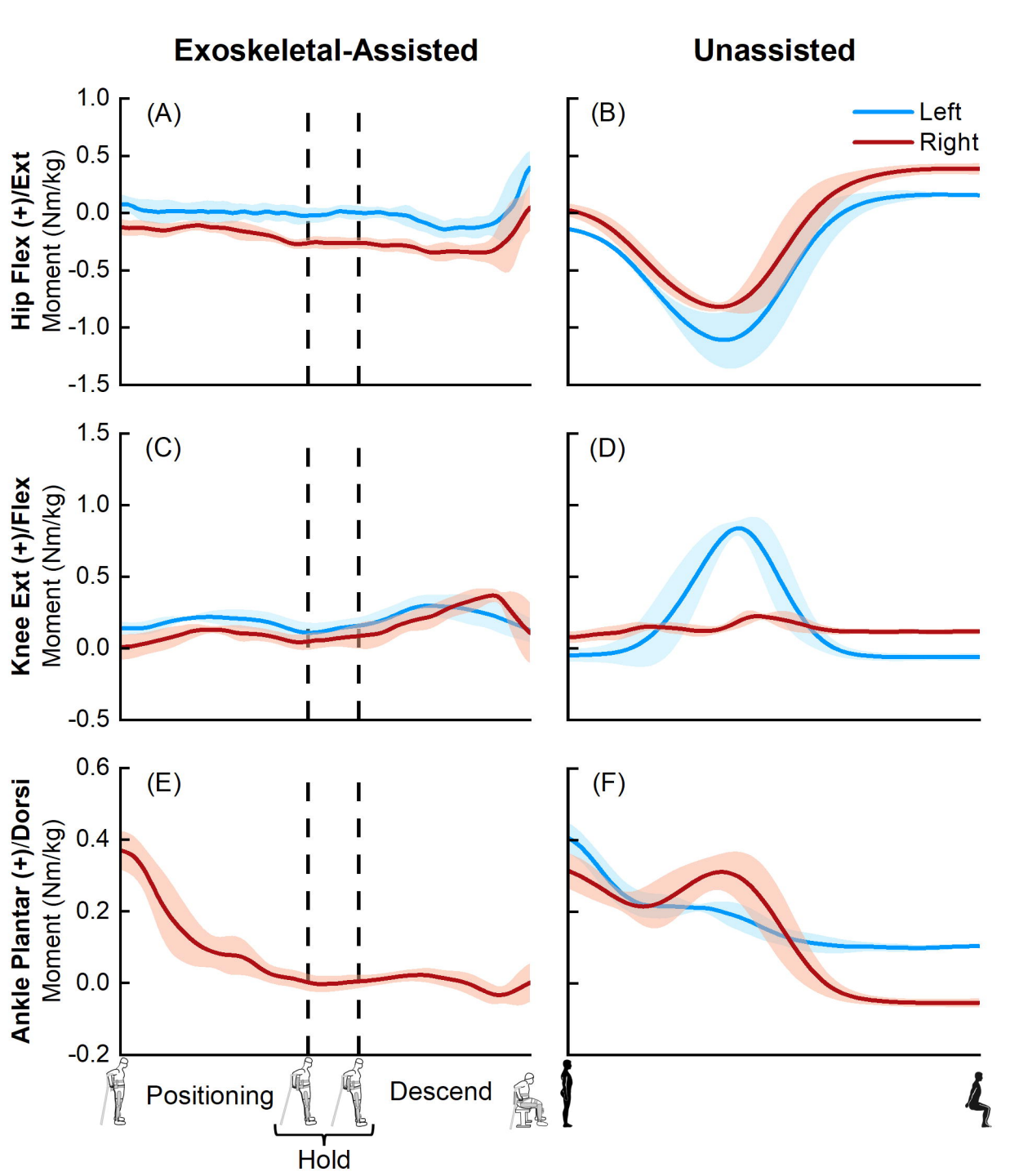
Exoskeletal-Assisted
Unassisted
(A)
(B)
(C)
(D)
(E)
(F)
Left
Right
Hip Flex (+)/Ext
Moment (Nm/kg)
Knee Ext (+)/Flex
Moment (Nm/kg)
Ankle Plantar (+)/Dorsi
Moment (Nm/kg)
1.0
0.5
0.0
-0.5
-1.0
-1.5
1.5
1.0
0.5
0.0
-0.5
0.6
0.4
0.2
0.0
-0.2
Positioning
Hold
Descend